



## Convection Initiation Caused by Heterogeneous Low-Level Jets over the Great Plains

JOSHUA G. GEBAUER

*School of Meteorology, and Cooperative Institute for Mesoscale Meteorological Studies,  
University of Oklahoma, Norman, Oklahoma*

ALAN SHAPIRO

*School of Meteorology, and Center for Analysis and Prediction of Storms, University of Oklahoma,  
Norman, Oklahoma*

EVGENI FEDOROVICH AND PETRA KLEIN

*School of Meteorology, University of Oklahoma, Norman, Oklahoma*

(Manuscript received 2 January 2018, in final form 12 June 2018)

### ABSTRACT

Observations from three nights of the Plains Elevated Convection at Night (PECAN) field campaign were used in conjunction with Rapid Refresh model forecasts to find the cause of north–south lines of convection, which initiated away from obvious surface boundaries. Such pristine convection initiation (CI) is relatively common during the warm season over the Great Plains of the United States. The observations and model forecasts revealed that all three nights had horizontally heterogeneous and veering-with-height low-level jets (LLJs) of nonuniform depth. The veering and heterogeneity were associated with convergence at the top-eastern edge of the LLJ, where moisture advection was also occurring. As time progressed, this upper region became saturated and, due to its placement above the capping inversion, formed moist absolutely unstable layers, from which the convergence helped initiate elevated convection. The structure of the LLJs on the CI nights was likely influenced by nonuniform heating across the sloped terrain, which led to the uneven LLJ depth and contributed toward the wind veering with height through the creation of horizontal buoyancy gradients. These three CI events highlight the importance of assessing the full three-dimensional structure of the LLJ when forecasting nocturnal convection over the Great Plains.

### 1. Introduction

The Great Plains region of the United States has long been known to have a nocturnal maximum in precipitation (Kincer 1916; Bleeker and Andre 1951; Wallace 1975; Easterling and Robinson 1985; Carbone and Tuttle 2008). This maximum is most pronounced in the months of June, July, and August, when nighttime precipitation exceeds daytime precipitation by 25% (Higgins et al. 1997). This nocturnal precipitation maximum is attributed to frequent nocturnal thunderstorms in the region. The thunderstorms are often elevated, in the sense that

storm updrafts develop in an elevated region separated from the surface by a nocturnal stable boundary layer (Colman 1990; Wilson and Roberts 2006).

One feature associated with the initiation and development of these nocturnal thunderstorms is the Great Plains low-level jet (LLJ) (Pitchford and London 1962; Maddox 1983; Astling et al. 1985; Trier and Parsons 1993; Trier et al. 2006; Tuttle and Davis 2006). LLJs are wind maxima that occur in the lowest levels of the atmosphere, typically within a kilometer of the ground. Blackadar (1957) showed that nocturnal LLJs can arise from an inertial oscillation that is triggered by the reduction of the friction force in the atmospheric boundary layer at sunset as thermally generated turbulence decays. The resulting force imbalance causes

---

*Corresponding author:* Joshua Gebauer, joshua.gebauer@ou.edu

DOI: 10.1175/MWR-D-18-0002.1

© 2018 American Meteorological Society. For information regarding reuse of this content and general copyright information, consult the [AMS Copyright Policy](http://www.ametsoc.org/PUBSReuseLicenses) ([www.ametsoc.org/PUBSReuseLicenses](http://www.ametsoc.org/PUBSReuseLicenses)).

the ageostrophic wind vector to rotate clockwise around the geostrophic wind vector with time. The maximum LLJ wind speed occurs when the ageostrophic wind vector aligns with the geostrophic wind vector. The inertial oscillation mechanism can produce nocturnal LLJs in practically any location, but climatological studies have found that LLJs in the United States are stronger and more frequent over the Great Plains (Bonner 1968; Walters et al. 2008). The strength and frequency of LLJs have been attributed to thermal effects associated with heating and cooling of the gentle slope (Holton 1967). This thermal forcing combined with the inertial oscillation produces stronger LLJs in this region (Bonner and Paegle 1970; Shapiro et al. 2016). Shapiro and Fedorovich (2009) established that thermally induced upslope and downslope motions over a shallow slope such as the Great Plains transform the inertial oscillation of Blackadar (1957) into an inertial-gravity oscillation. On the other hand, Parish (2016) suggested that the Great Plains LLJs are primarily controlled by the mean heating of the slope, which enhances the southerly geostrophic wind. It is likely that the effects described by Holton (1967), Shapiro and Fedorovich (2009), and Parish (2016) all contribute to the LLJ intensity and frequency maximum over the Great Plains.

The LLJ has long been considered to be a key contributor to the nocturnal precipitation maximum over the Great Plains, although not all mechanisms involved are well understood. A well-defined diurnal oscillation in moisture flux over the region is associated with the nocturnal LLJ (Rasmusson 1967; Higgins et al. 1997). Moist, warm air advected northward by the LLJ provides thermodynamic support for nocturnal elevated convection in the region. In addition to temperature and moisture advection, areas of convergence caused by the inhomogeneities of the LLJ can provide the dynamical support for convection. This support was statistically verified by Pitchford and London (1962), who found a significant correlation between convergence regions within the LLJ and thunderstorm location. Convergence often occurs at the northern terminus of the LLJ, so this region has received the bulk of the attention in studies of LLJ convergence in connection with thunderstorm initiation. The northern terminus of the LLJ has been found to be associated with heavy rainfall corridors (Astling et al. 1985; Trier et al. 2006; Tuttle and Davis 2006; Trier et al. 2014), as the convergence at the northern terminus of the LLJ provides low-level support for mesoscale convective systems (MCSs; Maddox 1980, 1983). The intersection between the LLJ and east-west-oriented atmospheric frontal boundaries can be

another region favorable for thunderstorm development (Trier and Parsons 1993).

While the northern terminus is often the region of strongest convergence within the LLJ, convergence can also be present in other regions. In an airflow configuration study by Walters and Winkler (2001), half of the identified LLJs had a wind direction that changed with height. This suggests that the position of convergence regions of these LLJs would vary with the orientation of the vertical shear vector. In fact, Walters and Winkler (2001) mention that there tends to be additional convection on the eastern side of LLJs associated with the more westerly wind direction at higher altitudes. In addition, the convergent regions of the LLJ are nonstationary. The veering of the LLJ with time can cause the convergent regions to shift as the night progresses. This shifting convergence can help to sustain thunderstorms after they move away from the initiation area, but it can also have the opposite effect of suppressing convection if the region of convergence moves away from the location of the storms and divergence develops (Bonner 1966). Changes in convergence with time are most evident on the flanks of the LLJ, with convergence decreasing on the western side of the LLJ throughout the night. At the same time, convergence increases on the eastern side owing to the clockwise turning of the ageostrophic wind in a horizontally heterogeneous LLJ (Bonner 1966).

Unfortunately, our current understanding of nocturnal convection initiation (CI), including the possible roles of LLJs, is incomplete. Accordingly, forecasting such CI over the Great Plains remains a difficult problem, particularly when the convection initiates away from a surface boundary or previous convection and in a region of the LLJ other than the northern terminus (so-called pristine CI). This latter type of CI, however, is relatively common for the Great Plains region. Reif and Bluestein (2017) showed that 24% of CI occurrences over the Great Plains are not associated with a boundary, and this no-boundary CI tends to occur in a north-south orientation on the eastern side of the LLJ late in the night (typically around 0900 UTC). The characteristics of these no-boundary CI events suggest that east-west heterogeneity of the LLJ may play a role in CI in such cases.

In this study, we analyze three episodes of nocturnal CI observed during the Plains Elevated Convection at Night (PECAN) field project (Geerts et al. 2017). In section 2, we discuss the data used in the analyses. The three cases are described in detail in section 3, and the cause of the observed LLJ structure and associated CI are discussed in section 4. Concluding remarks follow in section 5.

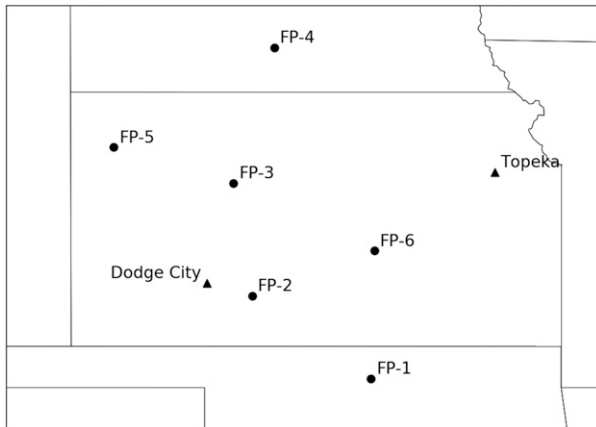


FIG. 1. Locations of the FPs (circles) and NWS sounding stations (triangles) over KS and neighboring states.

## 2. Methods

The PECAN project (Geerts et al. 2017) was designed to elucidate the processes contributing to the nocturnal precipitation maximum over the Great Plains. The PECAN field campaign ran from 1 June through 15 July 2015 and focused on four nocturnal phenomena: MCSs, CI, bores, and LLJs. The PECAN observing platforms included six fixed-location PECAN Integrated Sounding Arrays (PISAs), five mobile PISAs, three mobile radiosonde launch vehicles, multiple mobile mesonets, one fixed-location radar in addition to the regional WSR-88Ds, nine mobile radars, and three aircraft. Each PISA site provided vertical profiles of wind, temperature, and water vapor using both in situ and remote sensing observing platforms. During the field campaign, no-boundary CI with characteristics similar to those identified by Reif and Bluestein (2017) occurred on three nights: 1 June, 2 June, and 5 July 2015. On 1 and 2 June 2015, the CI did occur near previous convection, so it may not have met pristine CI criteria used by Reif and Bluestein (2017), but the orientation, position relative to the LLJ, and timing of the CI is similar to other no-boundary CI events. These three events were examined in the present study to determine the role of the LLJ in initiating the nocturnal CI.

Unfortunately, the three CI events considered in this study occurred on nights during which there was either no PECAN intensive operation period (IOP) or the PECAN IOP was focused on a region away from the CI. Since the mobile platforms were not positioned to observe these CI episodes, the best available observations were provided by the fixed PISAs (FPs). The coarse spacing of the fixed PISA sites (Fig. 1), however, was a limiting factor in the

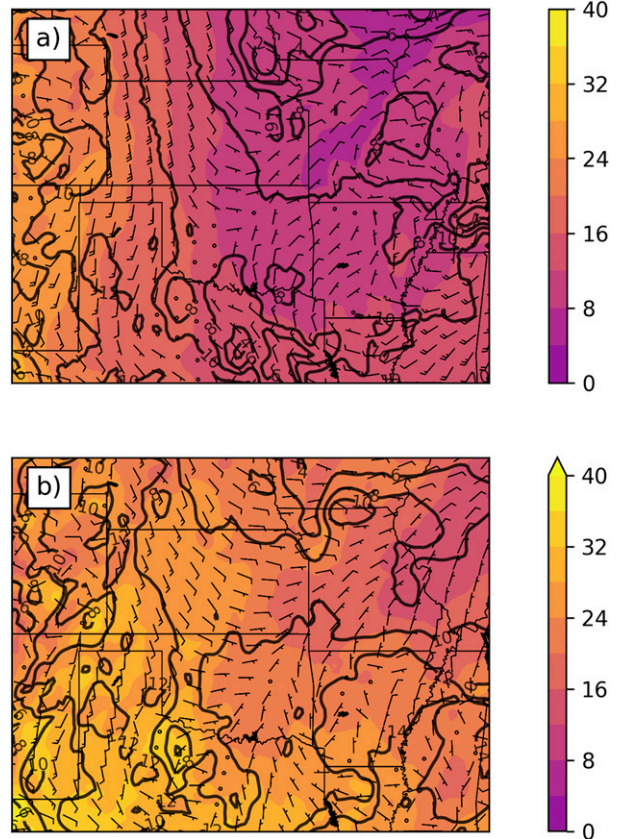


FIG. 2. Temperature ( $^{\circ}\text{C}$ ; shaded) and specific humidity ( $\text{g kg}^{-1}$ ; black contours) for (a) 850 hPa and (b) the surface over the Great Plains region from the 0000 UTC RAP analysis on 1 Jun 2015.

analyses of the selected events. For this reason, we decided to supplement the observations with numerical weather prediction (NWP) model data. Model forecasts were used instead of model analyses to avoid potential problems with discontinuous tendencies at analysis times.

On 1 and 2 June, NWP models used by the PECAN forecasters, such as the North American Mesoscale Forecast System (NAM), Rapid Refresh (RAP), High-Resolution Rapid Refresh (HRRR), and Colorado State 4-km WRF, had strong signals for no-boundary CI on the corresponding nights. Although these models did struggle with predicting convection on 5 July, they nevertheless produced some signal of CI in the correct location. One particular numerical model that showed skill at forecasting these CI events was the RAP model (Benjamin et al. 2016). The RAP has 13-km grid spacing and parameterized convection (Grell and Freitas 2014), so the fact that the RAP could forecast these no-boundary CI events was initially surprising. Wilson and Roberts (2006),

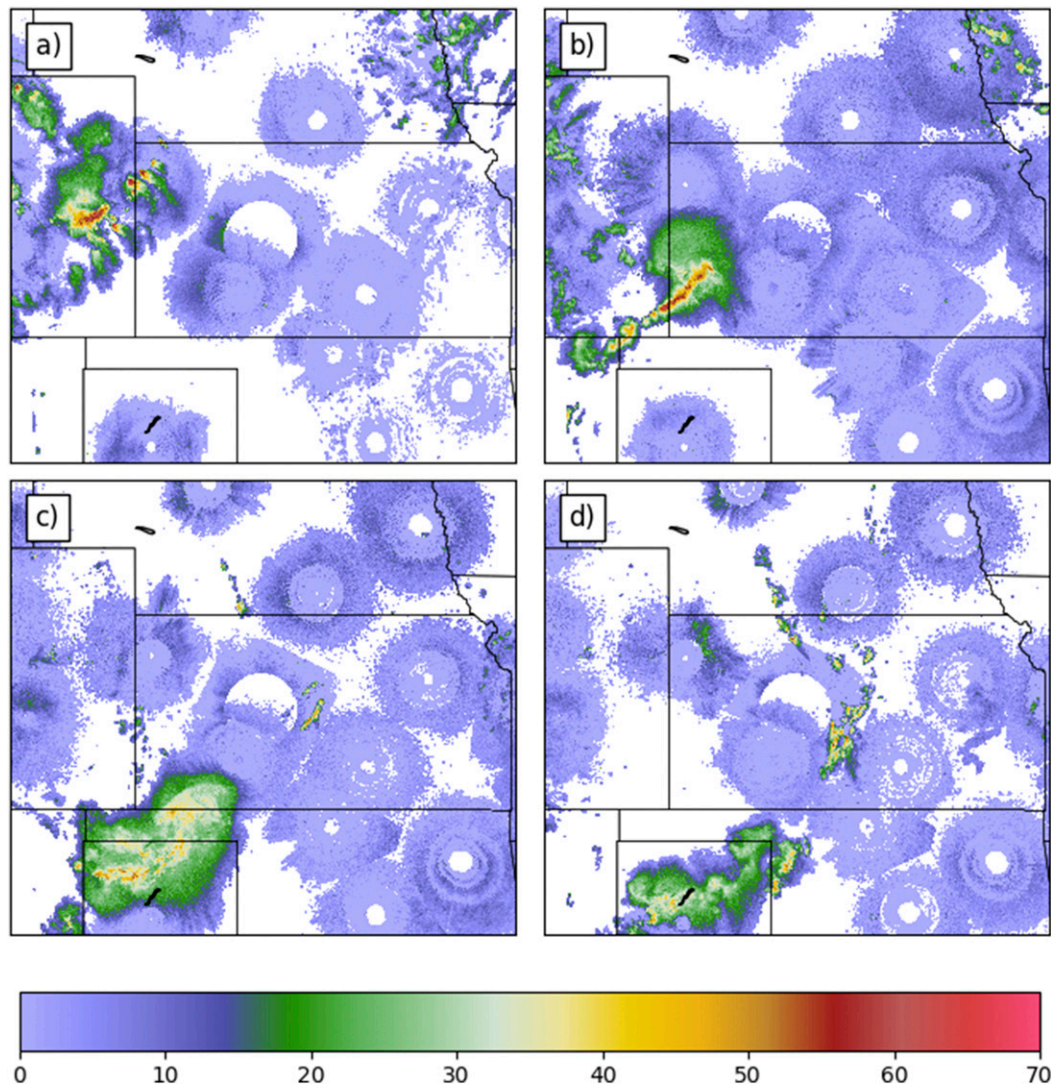


FIG. 3. Composite mosaic radar reflectivity on 1 Jun 2015 at (a) 0000, (b) 0330, (c) 0700, and (d) 0900 UTC. Composite mosaic radar data created by UCAR/NCAR–Earth Observing Laboratory (2016d).

however, showed that many of the convergent regions associated with elevated CI during the International H<sub>2</sub>O Project campaign (Weckwerth et al. 2004) over the southern Great Plains could be resolved on a 10-km analysis grid. While a 10-km grid spacing is slightly smaller than the 13-km grid spacing used by the RAP, this result does suggest that RAP parameterized convection may be used to help indicate the presence of mesoscale forcing likely to be supportive of the CI. However, a finer-scale, convection-allowing model (e.g., HRRR) may be necessary to identify the cloud-scale processes that potentially contribute to the considered CI events. Since the focus of this study is on the role of the LLJ in initiating convection initiation and not the cloud-scale processes, the RAP forecasts initialized

at 0000 UTC on the nights of the CI were used to analyze these nights.

### 3. Analysis of CI events

#### a. 1 June 2015

##### 1) SYNOPTIC AND RADAR OVERVIEW

Upper-air analysis for 0000 UTC 1 June 2015 indicates that the synoptic conditions over the Great Plains were unremarkable for convection. At 500 hPa, winds over the PECAN domain were northwesterly, with a trough located over southern Missouri and northern Arkansas and a ridge axis over the Colorado–Utah border. At 850 hPa, the winds over the western portion of the

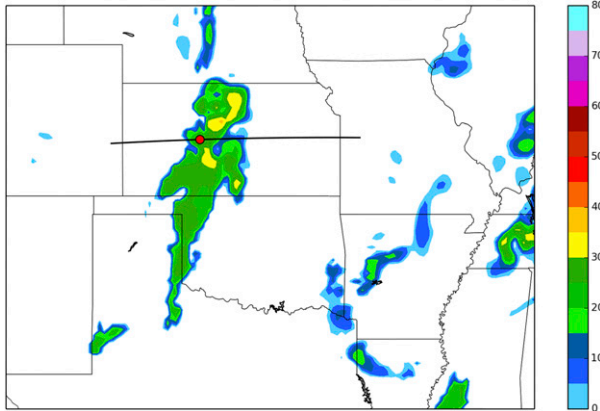


FIG. 4. Simulated composite reflectivity (dBZ) from the 0000 UTC 1 Jun 2015 RAP forecast valid for 1200 UTC. The black line indicates where the cross sections were taken. The red circle marks the location of the model soundings.

PECAN domain were southerly, but to the east, the winds at the 850-hPa surface underneath the 500-hPa trough were weak and variable (Fig. 2a). There was a ~12-K temperature difference between western and eastern Kansas at 850 hPa. The winds at 850 hPa, however, do not suggest that a frontal boundary is present. The westward increase of temperature on the 850-hPa surface in this region should be expected since the sloped terrain causes the 850-hPa surface to be much

closer to the ground in western Kansas than eastern Kansas. There was also a strong moisture gradient at 850 hPa over Kansas, with the specific humidity decreasing by  $6 \text{ g kg}^{-1}$  from west to east across the state. Close to the surface, the wind was southeasterly over western Kansas, but became weaker and turned to easterly over eastern Kansas. Horizontal gradients of temperature and moisture were also present at the surface, but they were less pronounced than at the 850-hPa level (Fig. 2b).

At 0000 UTC, scattered storms were present in eastern Colorado and northwestern Kansas (Fig. 3a). By 0330 UTC, the convection had consolidated into a northeast–southwest-oriented line of thunderstorms along the Colorado–Kansas border moving toward the south-southeast (Fig. 3b). Around 0700 UTC, convection began to develop in a north–south zone extending from central Kansas into south-central Nebraska (Fig. 3c). New convection continued to develop in this zone until 0900 UTC. After 0900 UTC, the convection drifted slowly toward the southeast and began to dissipate. The convergence at the top-eastern edge of the LLJ also moves eastward with time, and by 1200 UTC, the convergence region is near  $98^\circ\text{W}$  (Fig. 5d).

2) RAP FORECAST

The RAP forecast initialized at 0000 UTC for this night shows an elongated north–south zone of precipitation in

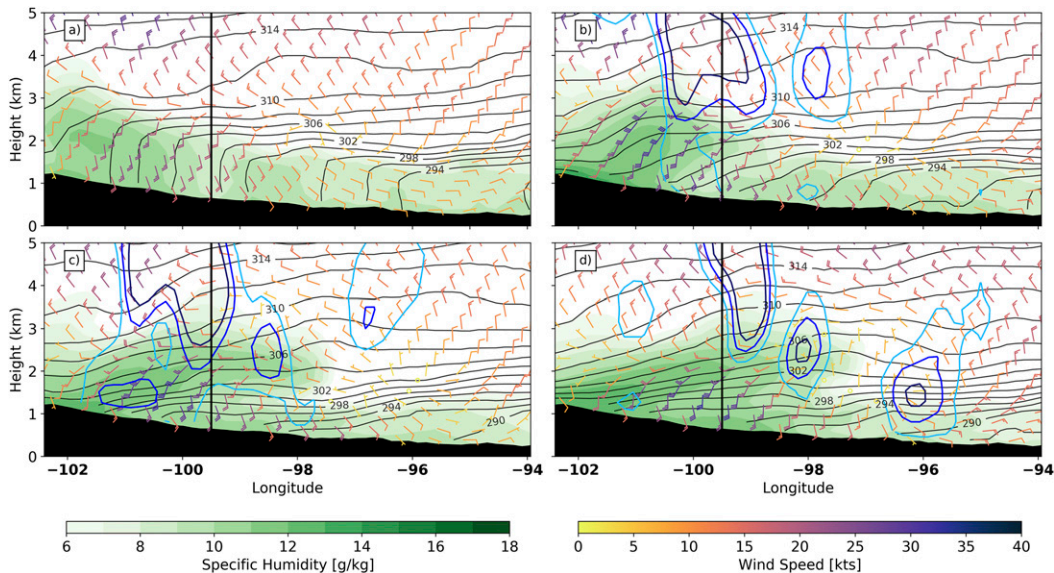


FIG. 5. Vertical cross sections of the 0000 UTC 1 Jun 2015 RAP forecast through the line indicated in Fig. 4 valid for (a) 0000, (b) 0400, (c) 0800, and (d) 1200 UTC. Potential temperature (K) is contoured. Specific humidity ( $\text{g kg}^{-1}$ ) greater than  $6 \text{ g kg}^{-1}$  is shaded in green. Wind speeds are in kt. A full barb is 10 kt, and a half barb is 5 kt. In (b)–(d), positive vertical velocity is contoured in blue, where light blue is  $1 \text{ cm s}^{-1}$ , medium blue is  $3 \text{ cm s}^{-1}$ , and dark blue is  $5 \text{ cm s}^{-1}$ . All heights are km MSL. The vertical black line shows the location of the model soundings.

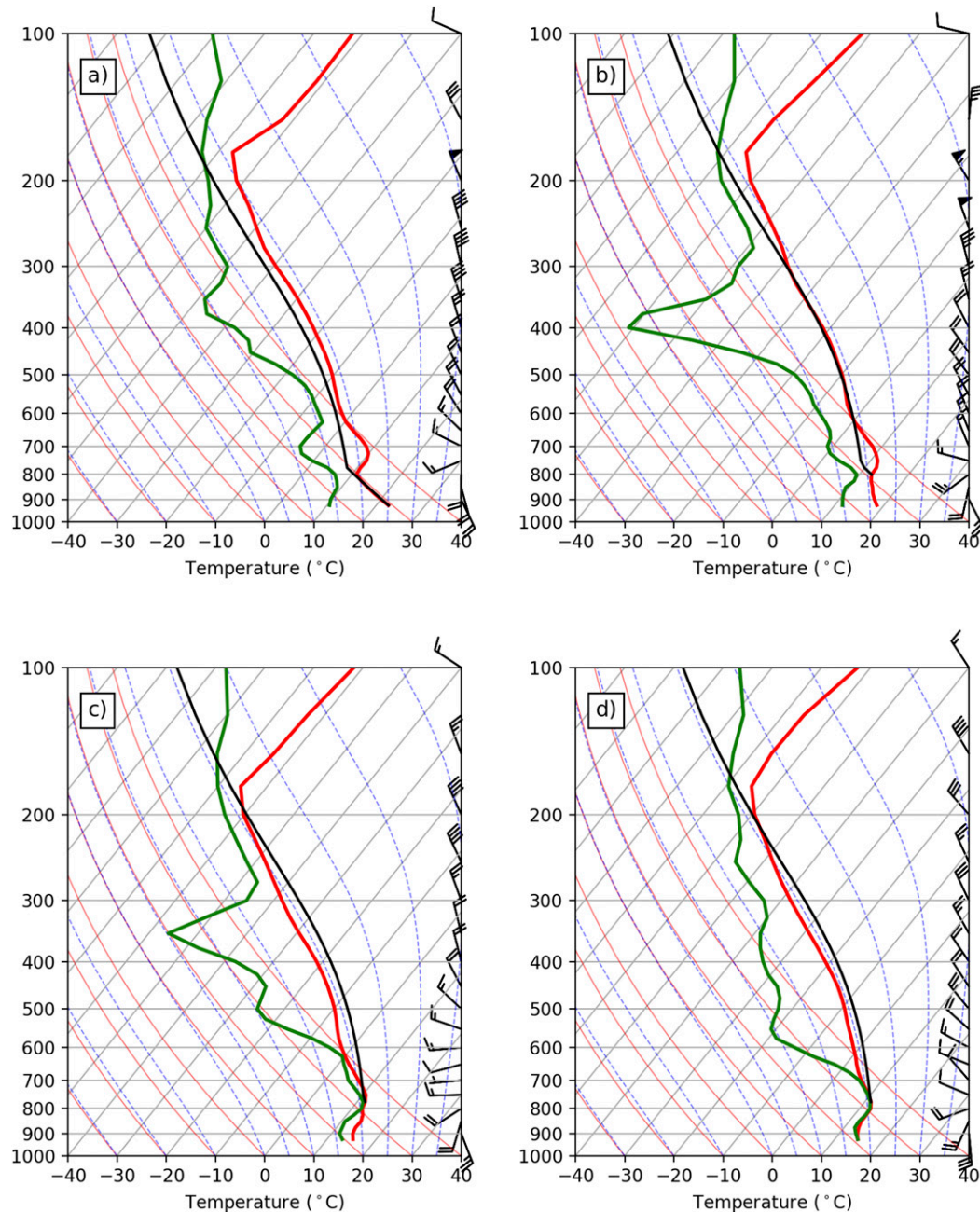


FIG. 6. Soundings from the RAP forecast initialized at 0000 UTC 1 Jun 2015 valid for (a) 0000, (b) 0400, (c) 0800, and (d) 1200 UTC at the location shown in Fig. 4. The black curve represents the ascent of the most unstable parcel.

the same area as the observed CI (Fig. 4). However, the north–south line of precipitation produced by the model lasts longer and has a more extensive spatial coverage than what was observed. Since the north–south orientation of the convection on these nights suggests that east–west heterogeneity of the LLJ might be important, east–west cross-sections of the RAP forecast were analyzed. At 0000 UTC, the isentropes show a convective boundary

layer with a deep mixed layer above the slope (Fig. 5a). The mixed layer generally tilts with the terrain but becomes deeper toward the west. By 0400 UTC in the forecast, a narrow, veering-with-height LLJ has developed. Associated with this veering is eastward advection of the moisture field at the top of the LLJ (Fig. 5b). In addition to the moisture advection, convergence of the  $u$ -wind field and rising motion is occurring at the top-eastern edge of

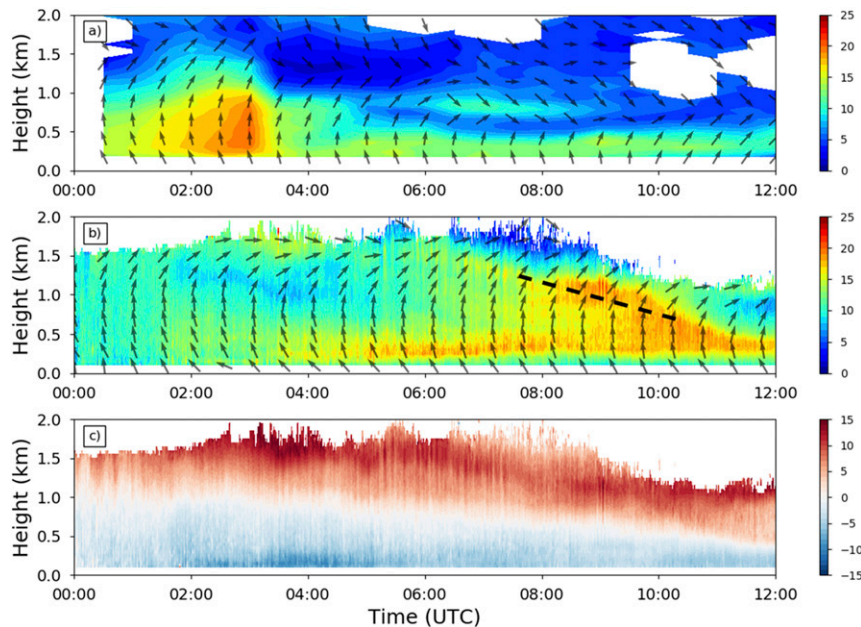


FIG. 7. (a) Time–height wind profile from the 915-MHz wind profiler at FP-5. The filled contours are wind speed ( $\text{m s}^{-1}$ ), and the black arrows are the horizontal wind direction. (b) As in (a), but for the Doppler lidar at FP-3. The black dashed line highlights the diagonal striation in wind speed. (c) The  $U$  component of the wind ( $\text{m s}^{-1}$ ) from the Doppler lidar at FP-3. Heights are in km AGL.

the LLJ around  $99^{\circ}$ – $100^{\circ}$ W longitude. The moisture advection continues throughout the night and results in the higher values of moisture, which were originally confined to western Kansas, to extend eastward above a stable layer in central Kansas. This location is where the model predicts the north–south line of precipitation (Fig. 5d).

RAP forecast soundings from the location where the model predicted the onset of the precipitation (as located by the red dot in Fig. 4) were examined to identify how the thermodynamic profile of the CI region was forecast to change throughout the night (Fig. 6). At 0000 UTC, the forecast profile is extremely stable with no convective available potential energy (CAPE), but by 0400 UTC, temperature and moisture advection occurring at the 800-hPa level have begun to change the profile. The moisture in this layer continues to increase through 0800 UTC, and at 1200 UTC in the forecast, the 775-hPa level is saturated with no convective inhibition (CIN). This layer could be classified as a moist absolutely unstable layer (MAUL; Bryan and Fritsch 2000). Trier et al. (2017) did not study the CI on this night but did show MAULs occurring on other nights during PECAN. These MAULs formed in areas of warm advection with mesoscale ascent.

The MAUL seen in this model sounding is likely embedded in a deeper layer that is being lifted by the mesoscale updraft created by the convergence at the

eastern edge of the LLJ. Without the mesoscale lifting, small-scale turbulence would likely cause the growth of small thermals from the MAUL due to the absolutely unstable condition. The mesoscale updraft, however, would help to support the growth of these localized updrafts. A combination of cloud-scale lift associated with the instability of the MAUL and lift from the mesoscale updraft created by the convergence associated with the LLJ likely caused the convection on these nights.

### 3) PECAN OBSERVATIONS

There were few PECAN observations available for 1 June 2015, as this was the first official night of the field campaign, and not all of the fixed PISA instruments were fully operating. Moreover, there was no IOP on this night, and thus, no coordinated soundings were conducted at the FP sites. Also, due to the limited east–west extent of the LLJ region on this night, only three of the fixed PISAs were located beneath the LLJ (and only two of these sites had an operational wind profiling instrument). Despite the lack of observational data, the upper-air wind data from two fixed PISA locations (FP-5 and FP-3) provided a glimpse of the LLJ structure and CI mechanism.

The LLJ was observed at FP-5 by a 915-MHz wind profiler (UCAR/NCAR–Earth Observing Laboratory 2016b)

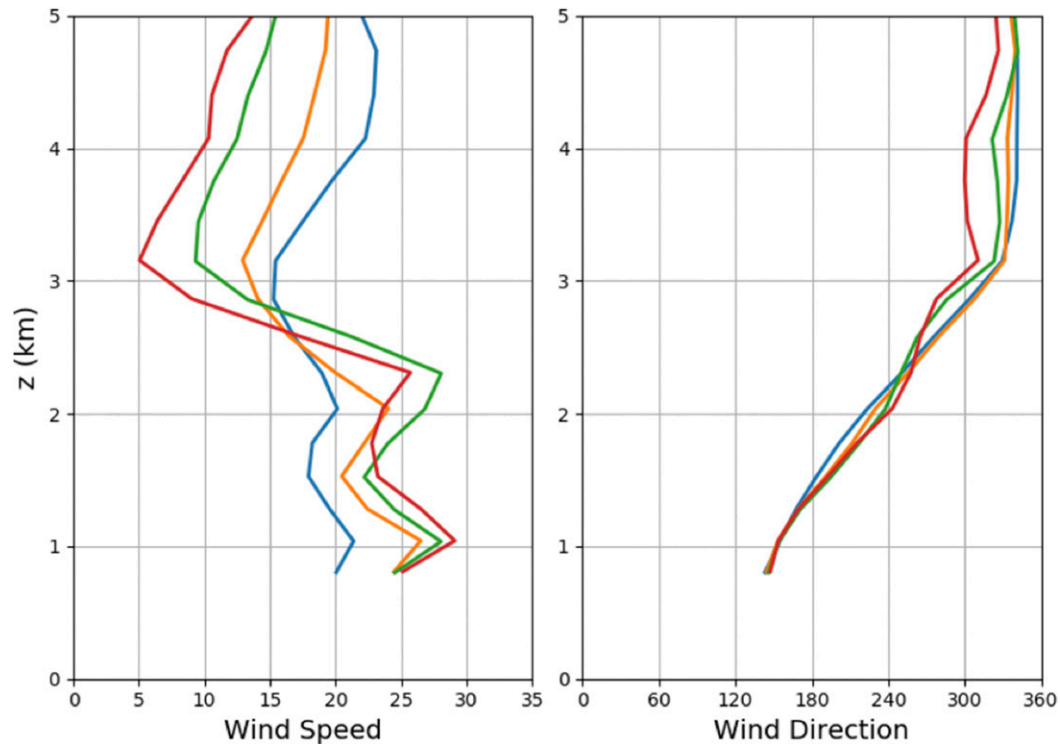


FIG. 8. Wind profiles at the edge of the LLJ located on the line shown in Fig. 4 at 0300 (blue), 0400 (orange), 0500 (green), and 0600 (red) UTC. Wind speed is in  $\text{m s}^{-1}$ , and height is km MSL.

and at FP-3 by a Doppler wind lidar (Hanesiak and Turner 2016). The evolution of the LLJ at the two sites was very different. At FP-5, the LLJ developed quickly and had wind speeds exceeding  $15 \text{ m s}^{-1}$  extending up to  $\sim 1 \text{ km}$  (Fig. 7a). The winds within this LLJ had the same veering-with-height structure that was seen in the RAP forecast. After 0300 UTC, the LLJ at FP-5 weakened and became shallower. It should be noted that storms directly south of FP-5 around this time may have interfered with the LLJ at this site. In contrast, the LLJ at FP-3 developed very slowly and remained shallow until 0800 UTC, when a diagonal striation (second wind maximum) appeared in the time–height wind profile around 1 km (Figs. 7b,c). A similar double wind maximum was also observed in the RAP forecast at the eastern edge of the LLJ (Fig. 8), which suggests that FP-3 was on the eastern edge of the LLJ. This second wind maximum was likely due to advection of the LLJ winds. In a veering-with-height LLJ, the top of the LLJ is advected eastward with time due to the westerly winds at that height. Therefore, locations on the eastern edge of such LLJs would observe a double wind maximum as LLJ winds that originate west of the location are advected over the location. As the night progressed, the middle levels of the LLJ acquired an increased westerly component, likely due to the inertial oscillation. This

resulted in the relative minimum in the wind speed profile on the eastern edge being eroded as the middle portion of the LLJ was advected eastward later on in the night.

A rough estimate of the east–west distance traveled by an air parcel at the top of the LLJ was calculated to determine if advection in a Lagrangian sense is a plausible explanation for the double wind maximum observed at FP-3. For an average  $u$  velocity of  $5 \text{ m s}^{-1}$  over 8 h, a parcel would travel 144 km to the east. This estimated distance traveled is close to the distance between FP-5 and FP-3. While this estimate is an upper bound to the distance traveled by an air parcel at the top of the LLJ, it does suggest that advection could create the observed double wind maximum.

This secondary wind maximum can also be used to identify convergence. Since the secondary wind maximum is associated with the eastern edge of the LLJ, one can infer that the convergence associated with the top-eastern edge of the LLJ must have been east of FP-3 by 0800 UTC. The time of the CI near FP-3 ( $\sim 0700 \text{ UTC}$ ) is slightly before the time when the strong second wind maximum appeared at FP-3, but the convergence from this secondary wind maximum likely contributed to the upscale growth in the convection seen in Fig. 3d. Both the RAP model forecast and the observations from the

fixed PISAs suggest that convergence on the top-eastern edge of the LLJ contributed to the development of the north–south line of convection that occurred on 1 June 2015.

### b. 2 June 2015

#### 1) SYNOPTIC AND RADAR OVERVIEW

The synoptic conditions on 2 June 2015 were analogous to those on 1 June 2015. In the PECAN domain, there was northwesterly flow at the 500-hPa surface, as the domain was situated between a ridge to the west and a trough to the east. On the 850-hPa surface, the winds over the western portion of the PECAN domain were southerly, but farther to the east, they were weak and variable. There was a  $\sim 6$ -K temperature decrease eastward across the region and a strong moisture gradient in eastern Kansas near the location of the CI (Fig. 9a). At the surface, the winds over far western Kansas were southeasterly with speeds around 15 kt ( $1 \text{ kt} = 0.5144 \text{ m s}^{-1}$ ), while over eastern Kansas, the winds were easterly with speeds of only 5 kt (Fig. 9b). Moisture values at the surface were higher than the previously described case, but as on 1 June 2015, there were no obvious synoptic-scale vertical motions on this night.

At 0000 UTC, scattered weak showers and thunderstorms were occurring in eastern Colorado, and a small MCS was present in the southern Nebraska panhandle (Fig. 10a). This storm moved toward the east-southeast and acquired the characteristics of a medium-to-large MCS by 0400 UTC (Fig. 10b). After this time, however, the storm weakened rapidly, and by 0800 UTC, only a stratiform region of precipitation remained. The MCS was a prolific producer of outflow boundaries, but for the most part, these boundaries did not initiate convection. A small north–south-oriented line of convection developed ahead of the stratiform region of precipitation around 1000 UTC (Fig. 10c). It appeared that the CI was occurring ahead of a southwest–northeast-oriented outflow boundary. The angle between the line of CI and the outflow boundary suggests that there was additional forcing, other than the outflow boundary, for CI in that north–south orientation. The main line of CI of interest for this study began to develop around 1100 UTC in a region well ahead of any radar-identified boundaries. This line also had a general north–south orientation and extended from southern Nebraska to southern Kansas (Fig. 10d).

#### 2) RAP FORECAST

As on 1 June 2015, the 0000 UTC RAP forecast for 2 June has a strong signal for CI in eastern Kansas at the

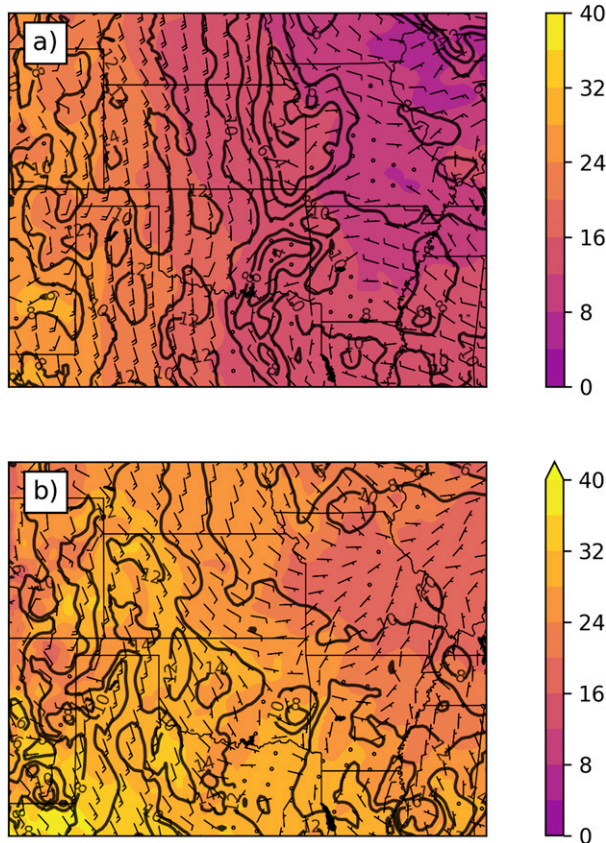


FIG. 9. As in Fig. 2, but for 2 Jun 2015.

correct time (Fig. 11). Interestingly, the MCS that developed along the Kansas–Nebraska border was not present in the RAP forecast. Since the RAP was predicting CI without the presence of the MCS, it is likely that the boundaries created by the MCS on that night were not the primary initiator of the north–south line of CI in eastern Kansas. The lack of prior convection in the RAP forecast made this model run particularly useful for identifying the cause of this no-boundary CI event.

East–west cross-sections of the modeled LLJ on 2 June 2015 were also examined. At 0000 UTC, the isentropes show the developed mixed layer. This layer is deeper and moister in western Kansas (Fig. 12a). By 0400 UTC, a veering-with-height LLJ develops over the western half of Kansas (Fig. 12b). This LLJ is broader than the LLJ on 1 June 2015, but both jets are similar in terms of their vertical structure. As on 1 June 2015, the veering of the LLJ with height is causing eastward moisture advection at the top of the LLJ. There is again a convergent region at the top-eastern edge of the LLJ, which initially is near  $97^{\circ}\text{W}$  longitude and moves eastward until 0800 UTC. The maximum convergence and moisture advection are occurring above a stable

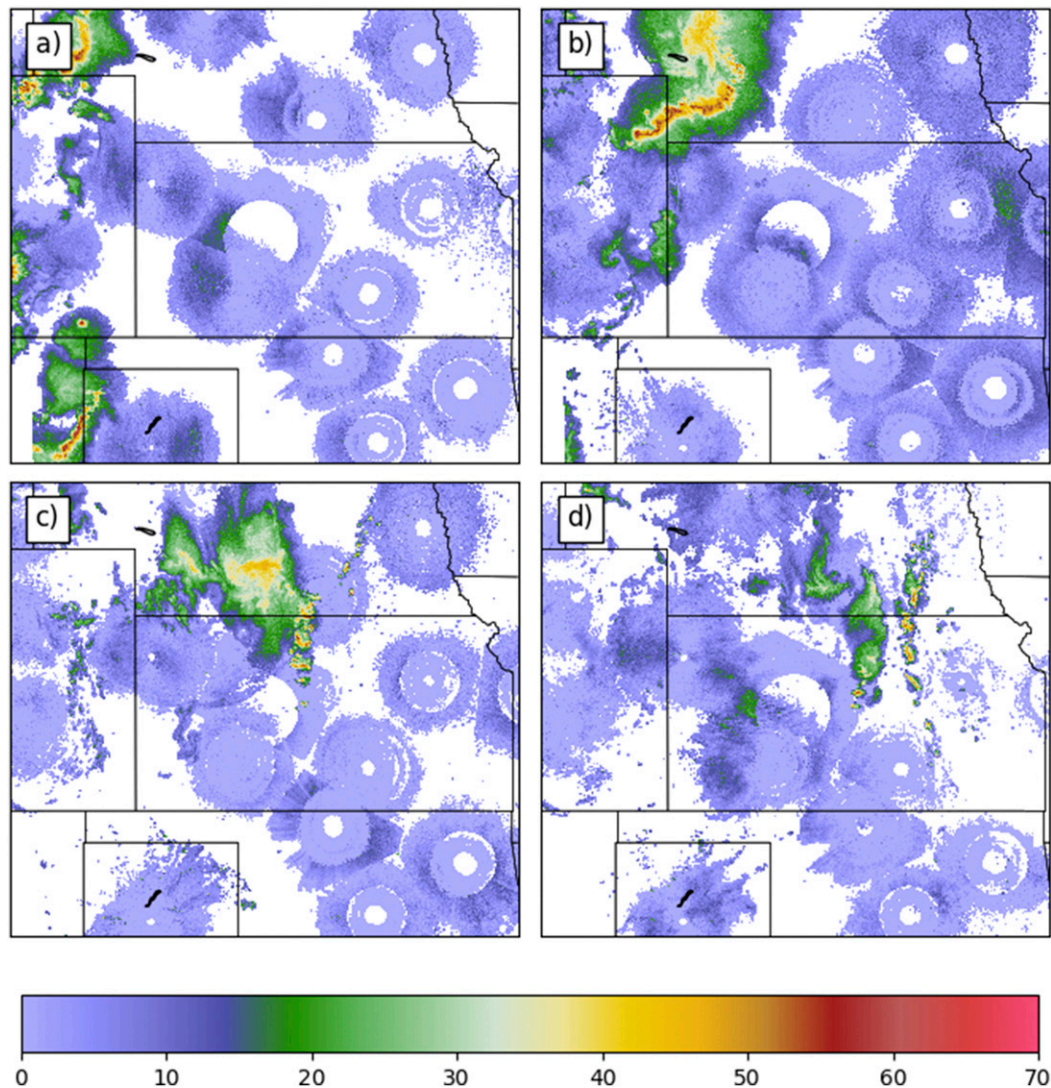


FIG. 10. Composite mosaic radar reflectivity on 2 Jun 2015 at (a) 0000, (b) 0500, (c) 0954, and (d) 1200 UTC.

layer, in a region where these two features are more likely to cause CI. The thickness of the LLJ is variable across the state, with the LLJ being deeper in western Kansas. This variability is creating additional convergent regions within the LLJ (for instance, around  $98^{\circ}\text{W}$ ; Fig. 12c). Finally, the RAP forecast for 1200 UTC shows that the peak moisture values that were initially in western Kansas moved eastward to the longitude of the model-predicted CI. Here, the convergence associated with the eastern edge of the LLJ is a likely trigger for the convection (Fig. 12d).

RAP model forecast soundings from the CI region on 2 June 2015 point to a similar thermodynamic profile evolution as on 1 June 2015 (Fig. 13). Initially, the profile is statically stable, but by 0400 UTC, significant moisture advection is occurring at the 800-hPa level. This

moisture advection continues throughout the night, and by 1200 UTC, a MAUL develops at 800–780 hPa. The convergence at the top-eastern edge of the LLJ could be a source of mesoscale lifting that helped initiates convection from this MAUL.

### 3) PECAN OBSERVATIONS

The IOP on 2 June 2015 was of short duration (it ended by 0500 UTC) and was merely a dry run for testing the mobile platforms' equipment. However, soundings were launched at all of the fixed PISA sites at 0300 UTC (Holdridge and Turner 2015; Vermeesch 2015; Clark 2016; UCAR/NCAR–Earth Observing Laboratory 2016c). These soundings allow the heterogeneity of the early-stage LLJ to be examined and provide an opportunity to check the accuracy of the

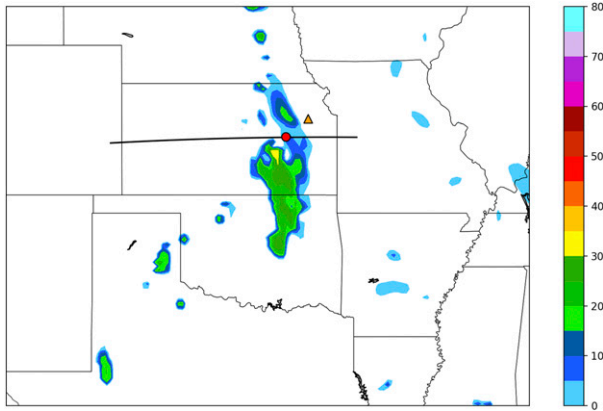


FIG. 11. As in Fig. 4, but for 2 Jun 2015. Additional orange triangle shows the location of the Topeka, KS, soundings on this night.

RAP forecast. Most instruments at the fixed PISA sites were also operating on this night.

The 0300 UTC soundings show spatial variability across Kansas, particularly between the western FP sites (FP-5, FP-3, and FP-2) and FP-6 (Fig. 14). The strength of the LLJ decreased toward the east, and at all locations, the LLJ wind direction veered with height. There were also higher moisture values in western Kansas. The soundings also show that the capping inversions strengthened toward the east. The FP-6 moisture profile suggests that an elevated moist layer was beginning to develop near the CI area at 0300 UTC. Unfortunately, since PECAN soundings were only taken once on this night, the temporal evolution of the LLJ heterogeneity and development of the elevated moisture layer was not

captured at the fixed PISA sites. The 0000 and 1200 UTC National Weather Service soundings from Topeka, Kansas, however, were useful in this regard. Topeka was located just to the east of the CI on this night and was also located slightly east of the RAP-forecast CI (see Fig. 11). The Topeka soundings provide the best representation of the thermodynamic profile of the CI region and can be used to identify how the environment was changing throughout the night. At 0000 UTC, the Topeka sounding was very stable, with a strong capping inversion at 850 hPa (Fig. 15). Above the capping inversion, an extremely dry layer extended up to 700 hPa. By 1200 UTC, the formerly dry layer was nearly saturated at 800 hPa, and the thermodynamic profile acquired a similar appearance to the RAP-forecast profile for the CI region. While there is no CAPE in this sounding, it is reasonable to assume that toward the west, the environment may have been more favorable for convection due to stronger mesoscale lifting in the region of eastward moisture transport. Notice, as at 0000 UTC, there was a capping inversion at 1200 UTC at 850 hPa, which indicates that the processes that formed the saturated layer occurred above 850 hPa. This is consistent with the RAP forecast showing eastward moisture advection occurring above the stable layer in eastern Kansas.

The fixed PISAs were not able to observe the eastern edge of this night’s LLJ since the jet was east of the PISAs, but remote sensing observations at FP-5 and FP-3 provide insights into the smaller north–south line of convection that developed to the east of the remnants from the MCS around 1000 UTC in the core of the

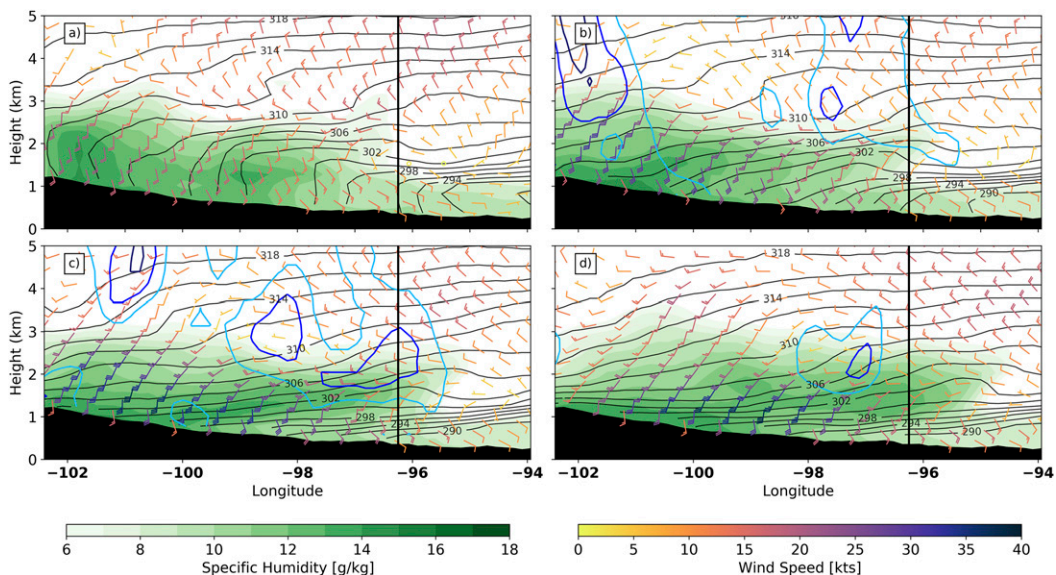


FIG. 12. As in Fig. 5, but for 2 Jun 2015. The times are (a) 0000, (b) 0400, (c) 0800, and (d) 1200 UTC.

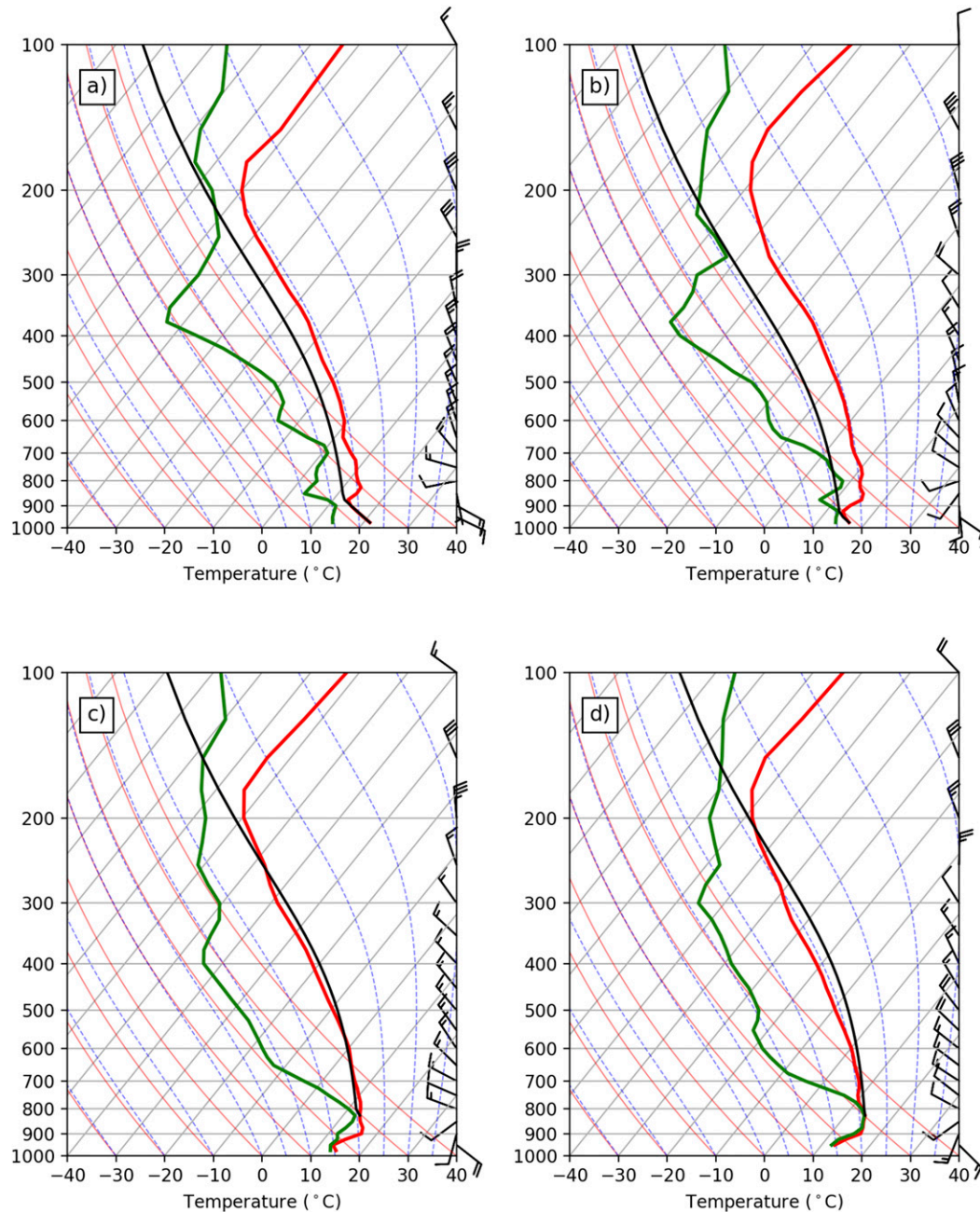


FIG. 13. Soundings from the RAP forecast initialized at 0000 UTC 2 Jun 2015 valid for (a) 0000, (b) 0400, (c) 0800, and (d) 1200 UTC at the locations shown in Fig. 11. The black curve represents the ascent of the most unstable parcel.

LLJ. Up until 0600 UTC, the LLJs at FP-5 and FP-3 had a similar evolution, with the LLJ at FP-5 slightly deeper and stronger than the LLJ at FP-3 (Fig. 16). After 0600 UTC, the wind profiler at FP-5 shows the LLJ became shallower and weakened before an apparent bore passed over the site around 0800 UTC (Fig. 16a). The Doppler lidar time–height profile at FP-3 shows a

diagonal striation in wind speed that began around 0600 UTC (Fig. 16b). Associated with this striation was also a slight change to a more westerly wind direction (Fig. 16c). The striation, while not as pronounced as the one seen on 1 June 2015 (Fig. 7), suggests that a region of elevated convergence passed over FP-3 around 0600 UTC. This convergence region is separate from

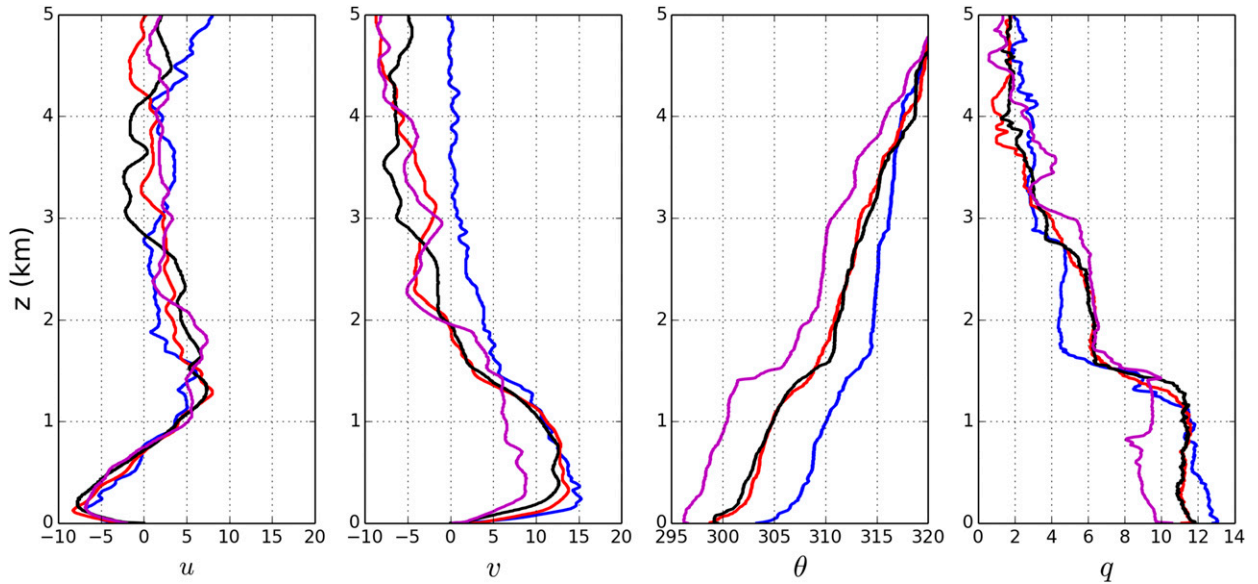


FIG. 14. Profiles of  $u$ ,  $v$ , potential temperature, and specific humidity from the 0300 UTC 2 Jun 2015 soundings at FP-5 (blue), FP-2 (red), FP-3 (black), and FP-6 (magenta). The vertical coordinate is km AGL.

the convergence zone at the eastern edge of the LLJ. The convergence region near FP-3 appears to be the result of the nonuniform LLJ depth. For a veering-with-height LLJ, a deeper LLJ to the west would create convergence in the westerly winds at the top of the LLJ at the eastern edge of the deeper portion of the LLJ. A similar feature was seen in the RAP forecast. The water vapor profile at FP-3 from the water vapor differential absorption lidar (DIAL; Spuler et al. 2015;

UCAR/NCAR–Earth Observing Laboratory 2016a) also indirectly suggests that a convergent region within the core of the LLJ was present (Fig. 17). A bulge in the depth of the moisture occurred around the same time as the secondary wind speed maximum observed on the lidar time–height profile (Fig. 17). This moisture bulge likely developed from the lift associated with the convergence. The two areas of extinguished signal around 0600 UTC suggest the formation of clouds, which is also

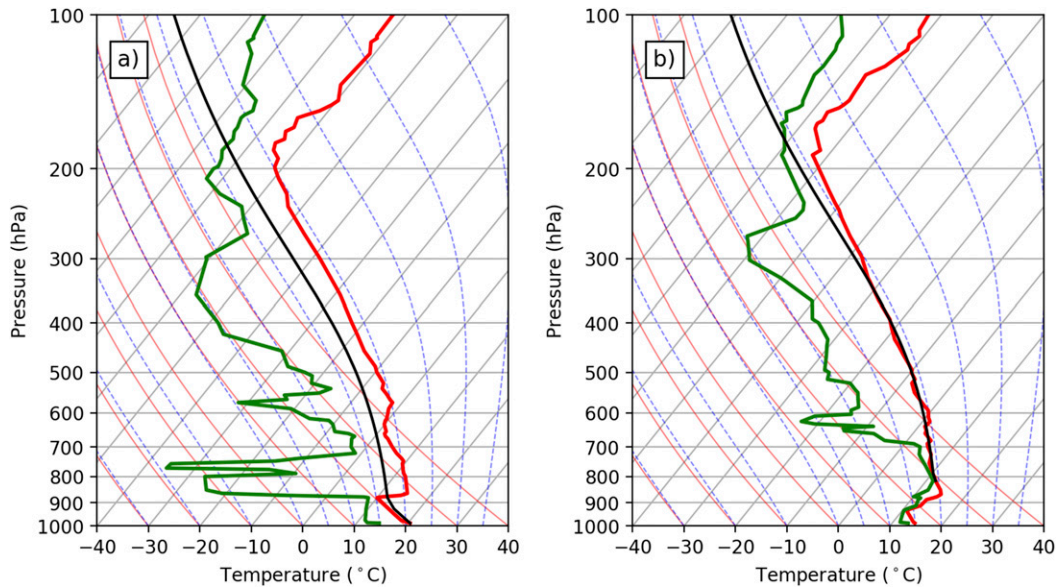


FIG. 15. The 0000 and 1200 UTC soundings for 2 Jun 2015 at Topeka, KS. The black line represents the most unstable parcel.

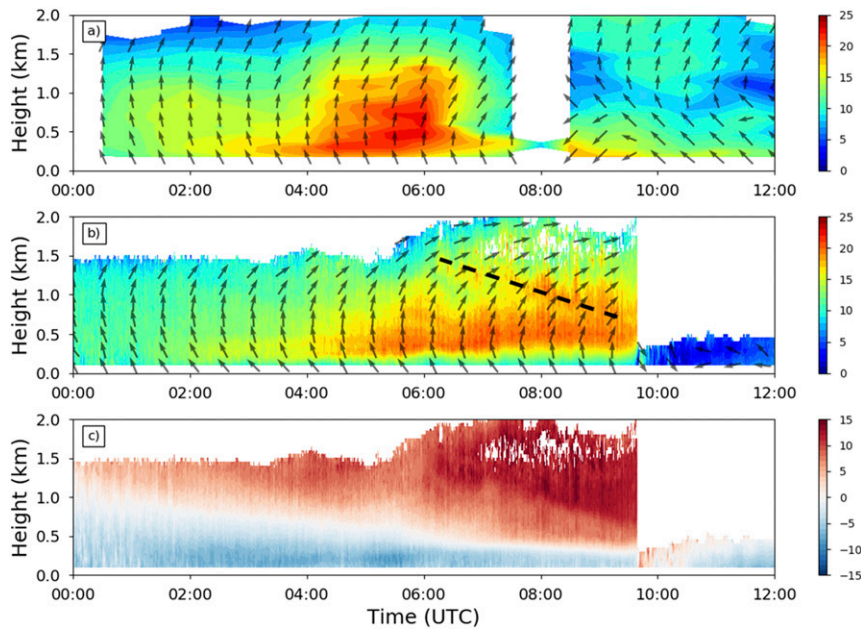


FIG. 16. As in Fig. 7, but for 2 Jun 2015.

consistent with convergence and rising motion occurring at this time. After 0600 UTC, the convergence region of the LLJ would have been east of FP-3, which aligns with timing and location of the small north–south line of CI. We hypothesize that the north–south line of CI closer to the MCS was due to the overlapping of the convergence region of the LLJ with the area of lift provided by the boundaries propagating from the decaying MCS.

### c. 5 July 2015

#### 1) SYNOPTIC AND RADAR OVERVIEW

The 5 July 2015 CI event has been discussed by Reif and Bluestein (2017) and Trier et al. (2017). Our present analysis suggests that the CI features reported in both papers were likely caused by a heterogeneous LLJ. On 5 July 2015, the synoptic pattern over the Great Plains was similar to the patterns observed on the two previously discussed nights. A ridge was located west of the region, while a trough was centered over the Mississippi Valley. Additionally, on this night, a small short-wave trough moved southeastward over eastern Kansas. Behind this trough, the synoptic forcing for convection was not particularly strong. Winds at 500 hPa were northwesterly over western Kansas and westerly over eastern Kansas. At 850 hPa, the winds were southerly over most of Kansas, with the strongest winds over western Kansas. There was again more moisture in western Kansas, and the horizontal temperature gradient at 850 hPa was stronger over western Kansas (Fig. 18a). At the surface,

the RAP analysis shows horizontally heterogeneous temperature and moisture fields, with both moisture and temperature generally increasing toward the west (Fig. 18b).

The 5 July 2015 night was noteworthy because of the three north–south lines of CI occurring away from a boundary. The first line of convection emerged around 0400 UTC, with a second line showing up slightly northeast of the first line  $\sim 3$  h later (Figs. 19b,c). The first two lines of CI were discussed by Reif and Bluestein (2017) and Trier et al. (2017). Around sunrise, a third, less vigorous and sparser north–south line of convection initiated in southeastern Kansas and northern Oklahoma (Fig. 19d). The separate north–south lines of convection initiated on this night suggest that the LLJ structure on this night was more complicated, with multiple convergence regions developing inside the LLJ.

#### 2) RAP FORECAST

The 0000 UTC RAP did not forecast these CI episodes as well as the CI episodes on the previously presented nights (Fig. 20). There is only a small hint of the first line of convection in western Kansas in the forecast, the second line of convection occurs too far to the east, and the third line of convection is not forecast. However, since the 0000 UTC RAP does indicate some signals for CI, it was still used to examine the structure of the forecast LLJ to see if key features of the LLJ were similar to those of LLJs on the other two nights. At 0000 UTC, the RAP shows a strong ( $\sim 20$  kt) decrease in wind speed eastward, but only a slight east–west

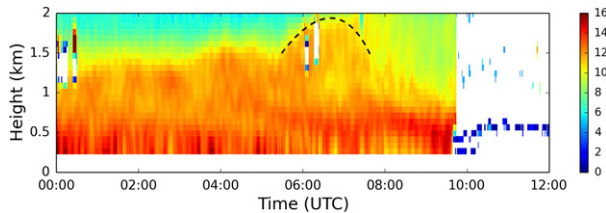


FIG. 17. Water vapor profile time series for 2 Jun 2015 from the water vapor DIAL located at FP-3. Values are  $\text{g m}^{-3}$ . The dashed black curve highlights the moisture bulge.

gradient in moisture (Fig. 21a). The late afternoon (0000 UTC) boundary layer is much deeper over western Kansas than over eastern Kansas. The LLJ depth at 0400 UTC varies across Kansas tremendously to a maximum of  $\sim 2$  km in western Kansas (Fig. 21b). This nonuniformly deep and strongly veering-with-height LLJ creates a region of convergence near  $100^\circ\text{W}$  longitude, which is approximately the location of the first line of the observed CI. Trier et al. (2017) also show convergence in the  $u$ -wind field at the location of the CI at 0600 UTC in their numerical simulation. By 0800 UTC (Fig. 21c), the LLJ depth is still uneven, but the disparity is not as prominent as at 0400 UTC. Eastward moisture advection occurs along the top of the LLJ in western Kansas, but it is not as significant as the other two nights due to the small moisture gradient. The convergence region and mesoscale updraft is now located from  $98^\circ$  to  $99^\circ\text{W}$ , which is where the model was predicting the second line of convection. At 1200 UTC, the edge of the nonuniform LLJ is located near  $98^\circ\text{W}$  longitude (Fig. 21d). Eastward moisture advection has contributed to the relatively deeper moisture region at this location.

Model soundings from the second line of CI were examined to identify if the thermodynamic profile evolution at the CI region was similar to the other two cases. At 0000 UTC, the profile is initially quite unstable with little CIN (Fig. 22a). The mixed layer extends up to the 750-hPa level, which is nearly saturated. At 0400 UTC, the environment has begun to stabilize, and the 750-hPa moisture has decreased (Fig. 22b). Significant moisture advection occurs at the 650-hPa level by 0800 UTC (Fig. 22c). While higher than what might be typically expected, this moisture advection is due to the LLJ. The 650-hPa level is typically around 3.5 km MSL. The model cross-section showed that the well-mixed boundary layer in western Kansas extended up to 3.5 km MSL, and the LLJ was shown to develop up to this height as well. The wind profile also indicates that a second wind maximum is present at the 650-hPa level. All of these features are consistent with the other two CI cases presented. Finally, at 1200 UTC, the level closest

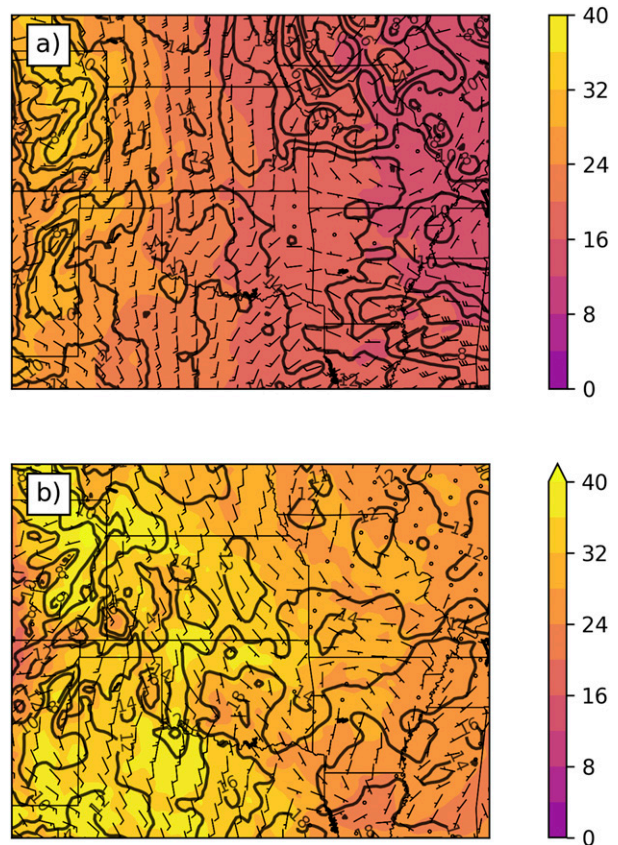


FIG. 18. As in Fig. 2, but for 5 Jul 2015.

to saturation has decreased in height to 700 hPa, and this level still has very little CIN (Fig. 22d).

### 3) PECAN OBSERVATIONS

The 5 July 2015 LLJ was the most well-observed LLJ of the three PECAN cases discussed in this paper. The IOP on this night was focused on bores in central Nebraska, so the mobile platforms were not in good positions to observe the LLJ and CI, but all of the wind-profiling instruments at the FP sites were operational. The wind profiler at FP-5 shows that the LLJ in western Kansas reached a depth of almost 2 km (Fig. 23a). What is most interesting, however, is that a diagonal striation in wind speed was observed around 0400 UTC. Analogous diagonal striations were also seen in lidar data at FP-3 on the other two nights presented. This diagonal striation began around the same time as the CI to the east of FP-5. As previously discussed for a veering-with-height LLJ, a diagonal striation in a time–height wind profile suggests that LLJ winds from the west were advected over the profiling site, with convergence apparent at the eastern edge of the stronger wind region. This striation agrees with the timing and location of the first

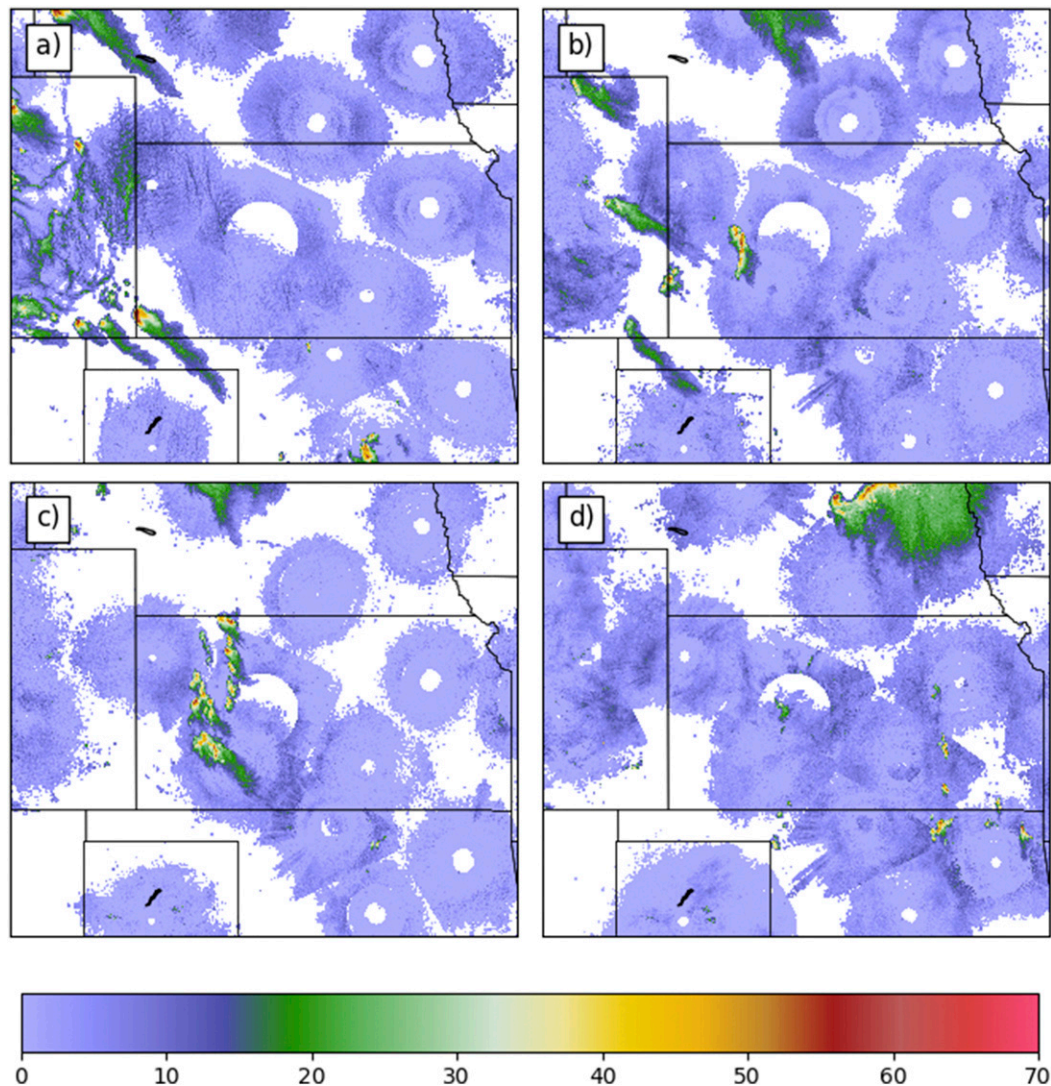


FIG. 19. Composite mosaic radar reflectivity on 5 Jul 2015 at (a) 0000, (b) 0430, (c) 0730, and (d) 1230 UTC.

line of CI on this night. Farther to the east, at FP-3, the LLJ was initially much shallower and weaker (Figs. 23b,c). This is in agreement with the RAP forecast, which predicted the LLJ to be stronger and deeper in western Kansas. Variability of the LLJ depth between FP-5 and FP-3 also suggests that there was a north–south convergence zone between FP-5 and FP-3 associated with the westerly winds at the top of the thicker LLJ in western Kansas.

The Doppler lidar at FP-6 in eastern Kansas shows an even shallower and weaker LLJ than at FP-3 (Fig. 24). A weak diagonal striation in the LLJ wind speed is evident at  $\sim 1100$  UTC. The LLJ acquired a more westerly wind direction when the diagonal striation appeared. The timing and location of this diagonal striation agrees with the timing and location of the weaker line of convection that initiated to the east of FP-6. It is unlikely that this

is the same convergence region that produced the first line of CI. It is more probable that there was a separate weaker convergence region inside this strongly heterogeneous LLJ.

#### 4. Discussion

##### a. Factors affecting the low-level jet

The CI cases considered in our paper were all associated with a veering-with-height LLJ, which had spatially nonuniform depth and wind speed. These horizontal and vertical variations resulted in convergence and differential moisture advection, which helped to initiate the convection. How did the LLJ acquire these features on the CI nights? One common feature noted on the RAP forecasts is a nonuniform

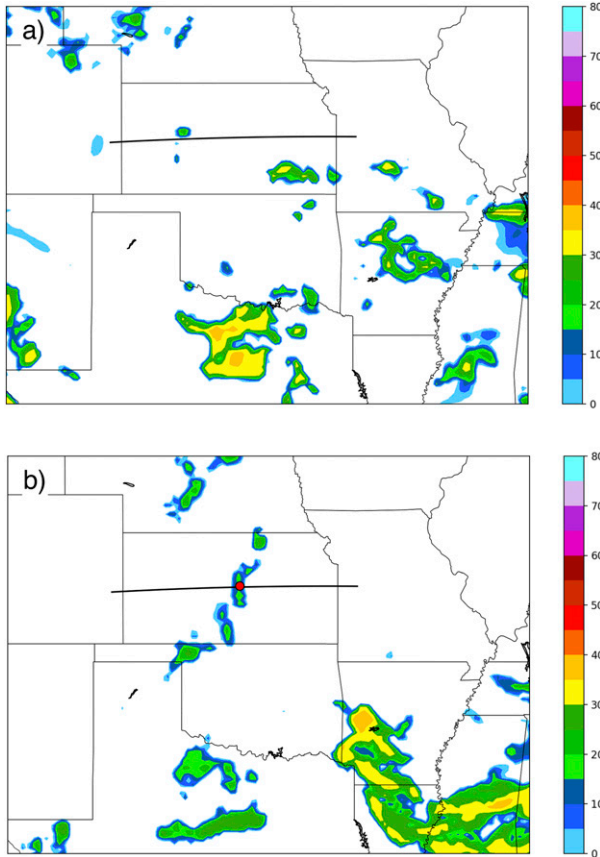


FIG. 20. Simulated composite reflectivity (dBZ) from the 0000 UTC 5 Jul 2015 RAP forecast valid for (a) 0400 and (b) 1000 UTC. The black line indicates where the cross sections were taken. The red circle marks the location of the model soundings.

mixed-layer depth across Kansas at 0000 UTC. The daytime mixed-layer depth can control the depth of the nocturnal LLJ. A deeper mixed layer subjects a deeper layer to a daytime frictional force due to more active turbulent transport of momentum, and therefore, a deeper layer would experience an inertial oscillation initiated by the decay of thermally generated turbulence around sunset. A deeper layer experiencing an inertial oscillation would produce a deeper LLJ.

The cause of the nonuniform mixed-layer depth requires more investigation. Since mixed-layer growth depends on thermally generated turbulence resulting from surface heating, the nonuniform mixed layer may have been caused by nonuniform surface heating. Without surface flux measurements, nonuniform heating cannot be proven with certainty; however, 2-m temperature data at FP-5 and FP-6 indicate that nonuniform heating may have occurred on all 3 days prior to the CI nights, as the diurnal potential temperature

increase at FP-5 is larger than that at FP-6 (Fig. 25). We hypothesize that uneven heating across Kansas contributed toward the nonuniform mixed-layer depth and, therefore, the nonuniform LLJ depth.

Nonuniform heating can also create the horizontally heterogeneous and veering winds in these LLJs. Multiple studies have suggested that the LLJ strength over the Great Plains is partially dependent on buoyancy values over the slope (Holton 1967; Shapiro and Fedorovich 2009; Shapiro et al. 2016; Gebauer et al. 2017). The nonuniform heating is indicative of these buoyancy values varying across the slope. The surface buoyancy gradients between FP-5 and FP-6 were calculated to quantify the buoyancy variation across the slope. To estimate the buoyancy gradient, one must work in a slope-following coordinate system where the  $x$  axis points down the slope, the  $y$  axis points northward, and the  $z$  axis points in the slope-normal direction, offset from the true vertical  $z^*$  by the slope angle  $\alpha$ . Buoyancy is defined as

$$b = \frac{g}{\theta_0}(\theta - \bar{\theta}), \tag{1}$$

where  $\theta$  is potential temperature,  $\bar{\theta}$  is the environmental potential temperature,  $g$  is gravity acceleration, and  $\theta_0$  is a reference value of potential temperature chosen as 300 K. The environmental potential temperature is described by

$$\bar{\theta} = \text{const} + \frac{\theta_0 N^2 z^*}{g}, \tag{2}$$

where  $N$  is the Brunt–Väisälä frequency (also known as buoyancy frequency), which we assume to be constant and define as  $N = \sqrt{(g/\theta_0)(\partial\bar{\theta}/\partial z^*)}$ . Taking  $\partial/\partial x$  of (1) and using (2) for  $\bar{\theta}$  (noting that  $\partial z^*/\partial x = -\sin\alpha$ ) then yields the downslope buoyancy gradient:

$$\frac{\partial b}{\partial x} = \frac{g}{\theta_0} \frac{\partial \theta}{\partial x} + N^2 \sin\alpha. \tag{3}$$

Previous studies have found that a typical tropospheric value of  $N$  tends to be around  $0.01 \text{ s}^{-1}$  (Tsuda et al. 1991; Revathy et al. 1996), so this value was used in our estimates. Figure 26 shows that the surface buoyancy gradient was negative on all three nights presented in this paper, with the magnitudes of the gradients weakening throughout the nights. Because of the LLJ's dependence on buoyancy, a negative buoyancy gradient would tend to produce LLJs that increased in intensity toward the west, which was a feature of the LLJs on the three CI nights.

The presence of a negative buoyancy gradient also explains the veering-with-height structure of these LLJs.

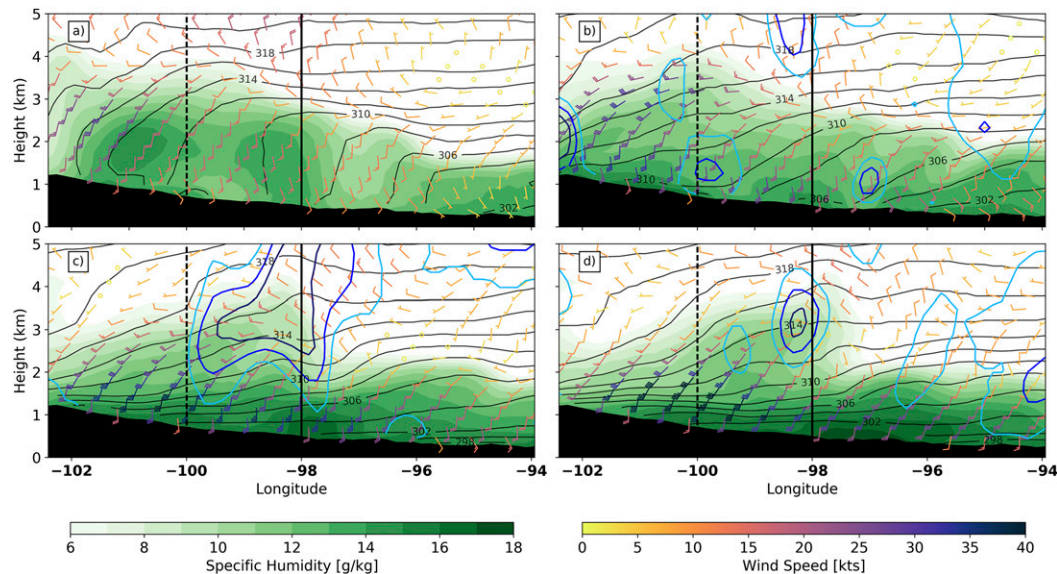


FIG. 21. As in Fig. 5, but for 5 Jul 2015. The times are (a) 0000, (b) 0400, (c) 0800, and (d) 1200 UTC. The dashed black line is the location of the first line of CI, and the solid black line is the location of the model soundings.

While an inertial oscillation of an Ekman profile produces a veering-with-height structure (Shapiro and Fedorovich 2010; see their Fig. 2), the veering seen on these nights exceeds that seen in the analytical studies. The negative buoyancy gradient present on these nights would generate positive horizontal vorticity in the  $y$  direction (vorticity vector points toward the north). Because of the vorticity generated by the buoyancy gradient, westerly shear would develop over the slope, which would contribute toward the veering with height of the LLJs.

Finally, the commonality of the synoptic pattern on these nights suggests that this pattern plays a role in these CI events. Notice that on all three nights, a 500-hPa trough was located to the east of the PECAN domain, and an amplifying 500-hPa ridge was to the west. As previously discussed, this synoptic pattern is not conducive to synoptic-scale vertical motions over the CI region. Instead, this synoptic pattern likely helped to enhance the buoyancy gradients over the slope, and as discussed above, LLJs that develop in the presence of a buoyancy gradient veer with height and are horizontally heterogeneous. In these cases, the PECAN domain was in a transition zone between cooler temperatures associated with the trough to the east and warm southerly return flow associated with the amplifying ridge to the west. This transition zone created an east–west buoyancy gradient across the slope. Figure 26 shows that a negative buoyancy gradient was present on 1 June and 4 July even before

diurnal heating, which is a sign that synoptic pattern was likely contributing to the buoyancy gradients on these days.

#### b. MAUL formation

One aspect of the considered CI cases that our study did not fully address is the formation of the MAULs on the nights with convection. Horizontal moisture advection alone is not sufficient to cause the CI area to become saturated since temperature advection also occurs simultaneously, and therefore the dewpoint depression would remain unchanged. Lift would be needed to adiabatically cool the air parcels as they were advected eastward. While the convergence zone at the top-eastern edge of the LLJ provides one source of lift near the CI region, it is possible that broad subtle lift was also occurring to the west within the core of the LLJs. The Trier et al. (2017) analysis of the 5 July CI event shows that persistent lift was occurring as parcels moved into the CI region, and the 1 June 2015 RAP forecast also showed persistent lift in the core of the LLJ. Reif and Bluestein (2017) suggest that warm air advection was the cause of the persistent vertical motion on 5 July 2015 due to its association with quasi-geostrophic ascent. There is no doubt that warm air advection was occurring within the LLJ on 5 July (and 1 and 2 June), but using warm air advection to diagnose vertical motion in highly ageostrophic flows such as LLJs appears questionable. More recently, Shapiro et al. (2018) presented a theory for gentle ascent in an

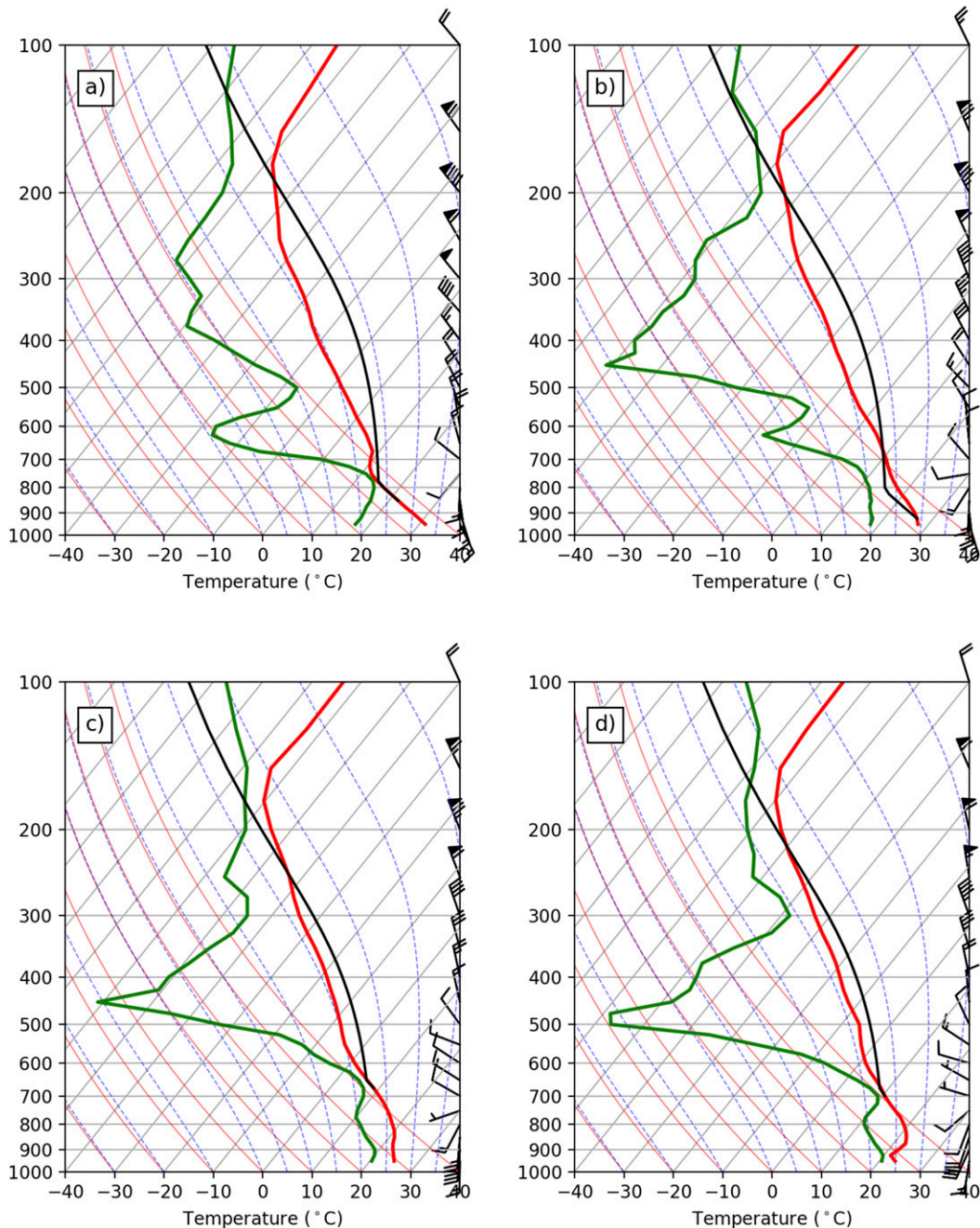


FIG. 22. Soundings from the RAP forecast initialized at 0000 UTC 5 Jul 2015 valid for (a) 0000, (b) 0400, (c) 0800, and (d) 1200 UTC at the locations shown in Fig. 20. The black curve represents the ascent of the parcel with the lowest amount of CIN.

LLJ as an inertia-gravity wave response to the shutdown of daytime mixing when a warm tongue is present in the convective boundary layer. Some semblance of a warm tongue was present on all three nights (westward increasing buoyancy); thus, Shapiro et al. (2018) applied their analytical model to LLJs on 2 June and 5 July. The model produced weak but persistent ascent

rates of  $\sim 4 \text{ cm s}^{-1}$  for these nights, which resulted in displacements exceeding 500 m. The vertical ascent rates produced by the Shapiro et al. (2018) mechanism are consistent with the MAUL formation on these nights. However, only the RAP forecast for 1 June 2015 indicates that persistent vertical motions were occurring in the core of the LLJ. A more detailed

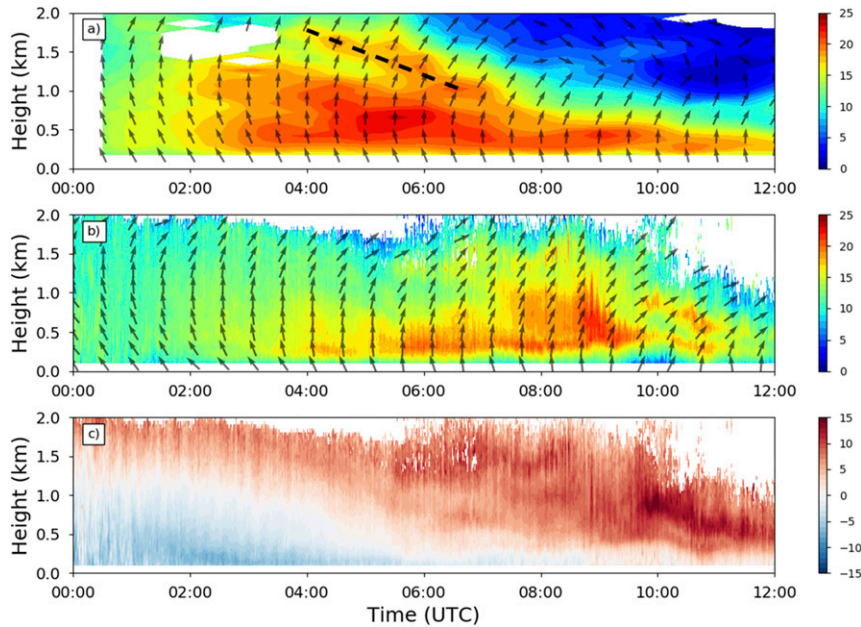


FIG. 23. As in Fig. 7, but for 5 Jul 2015. The dashed black line shows the diagonal striation in wind speed observed by the FP-5 wind profiler.

analysis of this subtle, albeit persistent, lift inside the LLJ is needed, as this may be a crucial process leading up to the initiation of convection in the presence of inhomogeneous LLJs.

## 5. Conclusions

One goal of the PECAN project was to better understand the role that nocturnal LLJs play in

elevated CI over the Great Plains. In this study, the LLJ was assessed as a potential contributor to CI in regions not associated with surface boundaries. Three such CI cases from PECAN were examined: 1 June, 2 June, and 5 July 2015. On all three nights, a horizontally heterogeneous, veering-with-height LLJ was present across the study area. Differential heating of the slope during the day and the resulting buoyancy gradients likely contributed to

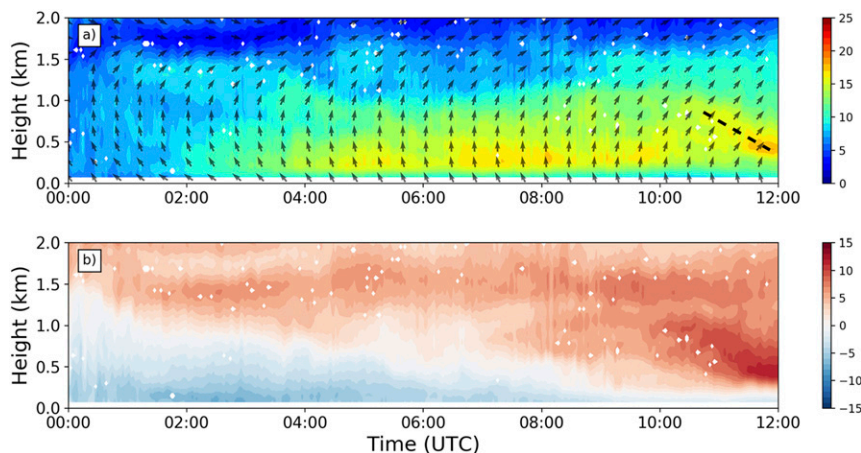


FIG. 24. (a) Time–height wind profile from the Doppler lidar at FP-6. The filled contours are wind speed ( $\text{m s}^{-1}$ ), and the black arrows are the horizontal wind direction. The dashed black line highlights the diagonal striation in wind speed. (b) The  $U$  component of the wind ( $\text{m s}^{-1}$ ) from the Doppler lidar at FP-6. Heights are in km AGL.

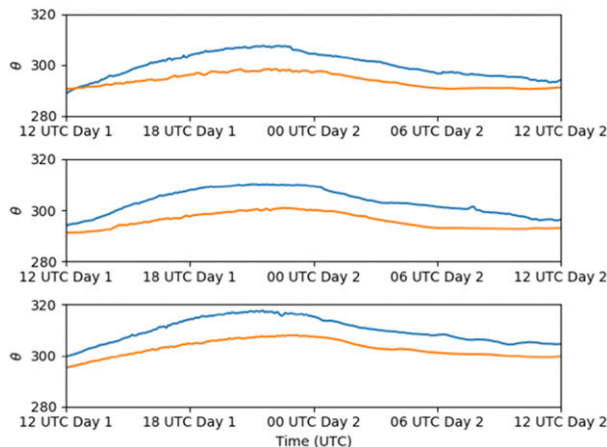


FIG. 25. The 2-m potential temperature at FP-5 (blue) and FP-6 (orange) for (top) 31 May–1 Jun, (middle) 1–2 Jun, and (bottom) 4–5 Jul 2015.

the observed structure of the LLJs on these nights. The LLJs were deeper and stronger in western Kansas, with the depth and intensity of the jets decreasing toward the east. As the LLJs evolved, the wind veering with height caused differential moisture advection across the LLJ axis. This moisture advection was a significant contributor to saturation at the top-eastern edge of the LLJ. The saturated region was located above the capping inversion in a layer with lower stability. In addition to the moisture advection, the heterogeneity in LLJ flow resulted in convergence of the  $u$ -wind field along the top-eastern edge of the LLJ. This convergence provided the lift that assisted in the initiation of the convection.

The commonality of the CI mechanisms in these cases shows the importance of evaluating the complete 3D structure of the LLJ when forecasting nocturnal convection over the Great Plains. In a highly ageostrophic flow such as the LLJ, horizontal and/or vertical variations of the LLJ winds can be critical for initiating vertical motions and ultimately triggering convection. Unfortunately, observing 3D variations in the LLJ flow fields is often difficult, and there is still much to learn about the Great Plains LLJ structure. For example, it is not known if the LLJ structural features and effect on the CI found on these three nights are typical for the Great Plains. If they are, what distinguishes the LLJs that cause the no-boundary CI from LLJs that do not? Understanding these and other features of the LLJ associated with CI could benefit from further studies that use observations in conjunction with numerical modeling.

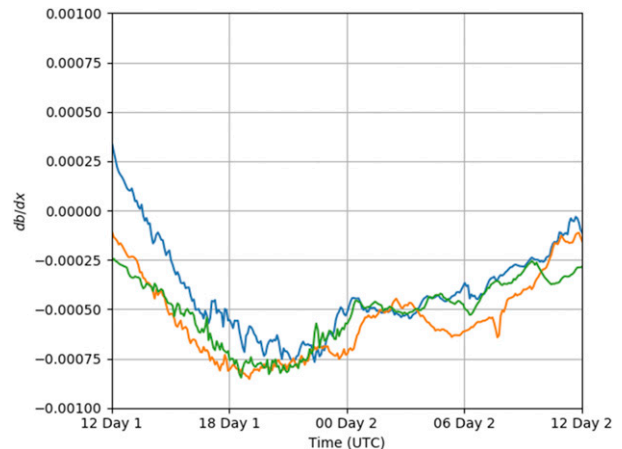


FIG. 26. Buoyancy gradient ( $\text{m s}^{-2} \text{km}^{-1}$ ) between FP-5 and FP-6 for 31 May–1 Jun (blue), 1–2 Jun (orange), and 4–5 Jul 2015 (green).

*Acknowledgments.* The authors thank Elizabeth Smith for her helpful comments and discussion. The authors also appreciate the hard work of all of the PECAN participants who helped collect and process data from the field campaign. Without them, this work would not be possible. This research was supported by the National Science Foundation under Grant AGS-1359698.

## REFERENCES

- Astling, E. G., J. Paegle, E. Miller, and C. J. O'Brien, 1985: Boundary layer control of nocturnal convection associated with a synoptic scale system. *Mon. Wea. Rev.*, **113**, 540–552, [https://doi.org/10.1175/1520-0493\(1985\)113<0540:BLCONC>2.0.CO;2](https://doi.org/10.1175/1520-0493(1985)113<0540:BLCONC>2.0.CO;2).
- Benjamin, S. G., and Coauthors, 2016: A North American hourly assimilation and model forecast cycle: The Rapid Refresh. *Mon. Wea. Rev.*, **144**, 1669–1694, <https://doi.org/10.1175/MWR-D-15-0242.1>.
- Blackadar, A. K., 1957: Boundary layer wind maxima and their significance for the growth of nocturnal inversions. *Bull. Amer. Meteor. Soc.*, **38**, 283–290.
- Bleeker, W., and M. J. Andre, 1951: On the diurnal variation of precipitation, particularly over the central U.S.A., and its relation to large-scale orographic circulation systems. *Quart. J. Roy. Meteor. Soc.*, **77**, 260–271, <https://doi.org/10.1002/qj.49707733211>.
- Bonner, W. D., 1966: Case study of thunderstorm activity in relation to the low-level jet. *Mon. Wea. Rev.*, **94**, 167–178, [https://doi.org/10.1175/1520-0493\(1966\)094<0167:CSOTAI>2.3.CO;2](https://doi.org/10.1175/1520-0493(1966)094<0167:CSOTAI>2.3.CO;2).
- , 1968: Climatology of the low level jet. *Mon. Wea. Rev.*, **96**, 833–850, [https://doi.org/10.1175/1520-0493\(1968\)096<0833:COTLLJ>2.0.CO;2](https://doi.org/10.1175/1520-0493(1968)096<0833:COTLLJ>2.0.CO;2).
- , and J. Paegle, 1970: Diurnal variations in boundary layer winds over the south-central United States in summer. *Mon. Wea. Rev.*, **98**, 735–744, [https://doi.org/10.1175/1520-0493\(1970\)098<0735:DVIBLW>2.3.CO;2](https://doi.org/10.1175/1520-0493(1970)098<0735:DVIBLW>2.3.CO;2).
- Bryan, G. H., and J. M. Fritsch, 2000: Moist absolute instability: The sixth static stability state. *Bull. Amer. Meteor. Soc.*, **81**, 1207–1230, [https://doi.org/10.1175/1520-0477\(2000\)081<1287:MAITSS>2.3.CO;2](https://doi.org/10.1175/1520-0477(2000)081<1287:MAITSS>2.3.CO;2).

- Carbone, R. E., and J. D. Tuttle, 2008: Rainfall occurrence in the U.S. warm season: The diurnal cycle. *J. Climate*, **21**, 4132–4146, <https://doi.org/10.1175/2008JCLI2275.1>.
- Clark, R., 2016: FP3 Ellis, KS radiosonde data, version 2.0. UCAR/NCAR–Earth Observing Laboratory, accessed 5 October 2016, <https://doi.org/10.5065/D6GM85DZ>.
- Colman, B. R., 1990: Thunderstorms above frontal surfaces in environments without positive CAPE. Part I: A climatology. *Mon. Wea. Rev.*, **118**, 1103–1122, [https://doi.org/10.1175/1520-0493\(1990\)118<1103:TAFSIE>2.0.CO;2](https://doi.org/10.1175/1520-0493(1990)118<1103:TAFSIE>2.0.CO;2).
- Easterling, D. R., and P. J. Robinson, 1985: The diurnal variation of thunderstorm activity in the United States. *J. Climate Appl. Meteor.*, **24**, 1048–1058, [https://doi.org/10.1175/1520-0450\(1985\)024<1048:TDTVOTA>2.0.CO;2](https://doi.org/10.1175/1520-0450(1985)024<1048:TDTVOTA>2.0.CO;2).
- Gebauer, J. G., E. Fedorovich, and A. Shapiro, 2017: A 1D theoretical analysis of northerly low-level jets over the Great Plains. *J. Atmos. Sci.*, **74**, 3419–3431, <https://doi.org/10.1175/JAS-D-16-0333.1>.
- Geerts, B., and Coauthors, 2017: The 2015 Plains Elevated Convection at Night field project. *Bull. Amer. Meteor. Soc.*, **98**, 767–786, <https://doi.org/10.1175/BAMS-D-15-00257.1>.
- Grell, G. A., and S. R. Freitas, 2014: A scale and aerosol aware stochastic convective parameterization for weather and air quality modeling. *Atmos. Chem. Phys.*, **14**, 5233–5250, <https://doi.org/10.5194/acp-14-5233-2014>.
- Hanesiak, J., and D. Turner, 2016: FP3 University of Manitoba Doppler lidar wind profile data, version 1.0. UCAR/NCAR–Earth Observing Laboratory, accessed 30 January 2017, <https://doi.org/10.5065/D60863P5>.
- Higgins, R., Y. Yao, E. Yarosh, J. Janowiak, and K. Mo, 1997: Influence of the Great Plains low-level jet on summertime precipitation and moisture transport over the central United States. *J. Climate*, **10**, 481–507, [https://doi.org/10.1175/1520-0442\(1997\)010<0481:IOTGPL>2.0.CO;2](https://doi.org/10.1175/1520-0442(1997)010<0481:IOTGPL>2.0.CO;2).
- Holdridge, D., and D. Turner, 2015: FP6 Hesston, KS radiosonde data, version 1.0. UCAR/NCAR–Earth Observing Laboratory, accessed 5 March 2016, <https://doi.org/10.5065/D6765CD0>.
- Holton, J. R., 1967: The diurnal boundary layer wind oscillation above sloping terrain. *Tellus*, **19**, 199–205, <https://doi.org/10.1111/j.2153-3490.1967.tb01473.x>.
- Kincer, J. B., 1916: Daytime and nighttime precipitation and their economic significance. *Mon. Wea. Rev.*, **44**, 628–633, [https://doi.org/10.1175/1520-0493\(1916\)44<628:DANPAT>2.0.CO;2](https://doi.org/10.1175/1520-0493(1916)44<628:DANPAT>2.0.CO;2).
- Maddox, R. A., 1980: Mesoscale convective complexes. *Bull. Amer. Meteor. Soc.*, **61**, 1374–1400, [https://doi.org/10.1175/1520-0477\(1980\)061<1374:MCC>2.0.CO;2](https://doi.org/10.1175/1520-0477(1980)061<1374:MCC>2.0.CO;2).
- , 1983: Large-scale meteorological conditions associated with midlatitude, mesoscale convective complexes. *Mon. Wea. Rev.*, **111**, 1475–1493, [https://doi.org/10.1175/1520-0493\(1983\)111<1475:LSMCAW>2.0.CO;2](https://doi.org/10.1175/1520-0493(1983)111<1475:LSMCAW>2.0.CO;2).
- Parish, T. R., 2016: A comparative study of 3 June 2015 Great Plains low-level jet. *Mon. Wea. Rev.*, **144**, 2963–2979, <https://doi.org/10.1175/MWR-D-16-0071.1>.
- Pitchford, K. L., and J. London, 1962: The low-level jet as related to nocturnal thunderstorms over Midwest United States. *J. Appl. Meteor.*, **1**, 43–47, [https://doi.org/10.1175/1520-0450\(1962\)001<0043:TLLJAR>2.0.CO;2](https://doi.org/10.1175/1520-0450(1962)001<0043:TLLJAR>2.0.CO;2).
- Rasmusson, E. M., 1967: Atmospheric water vapor transport and the water balance of North America. Part I: Characteristics of the water vapor flux field. *Mon. Wea. Rev.*, **95**, 403–426, [https://doi.org/10.1175/1520-0493\(1967\)095<0403:AWVTAT>2.3.CO;2](https://doi.org/10.1175/1520-0493(1967)095<0403:AWVTAT>2.3.CO;2).
- Reif, D. W., and H. B. Bluestein, 2017: A 20-year climatology of nocturnal convection initiation over the central and southern Great Plains during the warm season. *Mon. Wea. Rev.*, **145**, 1615–1639, <https://doi.org/10.1175/MWR-D-16-0340.1>.
- Revathy, K., S. R. Prabhakaran Nair, and B. V. Krishna Murthy, 1996: Deduction of temperature profile from MST radar observations of vertical wind. *Geophys. Res. Lett.*, **23**, 285–288, <https://doi.org/10.1029/96GL00086>.
- Shapiro, A., and E. Fedorovich, 2009: Nocturnal low-level jets over a shallow slope. *Acta Geophys.*, **57**, 950–980, <https://doi.org/10.2478/s11600-009-0026-5>.
- , and —, 2010: Analytical description of a nocturnal low-level jet. *Quart. J. Roy. Meteor. Soc.*, **136**, 1255–1262, <https://doi.org/10.1002/qj.628>.
- , —, and S. Rahimi, 2016: A unified theory for the Great Plains nocturnal low-level jet. *J. Atmos. Sci.*, **73**, 3037–3057, <https://doi.org/10.1175/JAS-D-15-0307.1>.
- , —, and J. G. Gebauer, 2018: Mesoscale ascent in nocturnal low-level jets. *J. Atmos. Sci.*, **75**, 1403–1427, <https://doi.org/10.1175/JAS-D-17-0279.1>.
- Spuler, S. M., K. S. Repasky, B. Morley, D. Moen, M. Hayman, and A. R. Nehrir, 2015: Field-deployable diode-laser-based differential absorption lidar (DIAL) for profiling water vapor. *Atmos. Meas. Tech.*, **8**, 1073–1087, <https://doi.org/10.5194/amt-8-1073-2015>.
- Trier, S. B., and D. B. Parsons, 1993: Evolution of environmental conditions preceding the development of a nocturnal mesoscale convective complex. *Mon. Wea. Rev.*, **121**, 1078–1098, [https://doi.org/10.1175/1520-0493\(1993\)121<1078:EOECPT>2.0.CO;2](https://doi.org/10.1175/1520-0493(1993)121<1078:EOECPT>2.0.CO;2).
- , C. A. Davis, D. A. Ahijevych, M. L. Weisman, and G. H. Bryan, 2006: Mechanisms supporting long-lived episodes of propagating nocturnal convection within a 7-day WRF Model simulation. *J. Atmos. Sci.*, **63**, 2437–2461, <https://doi.org/10.1175/JAS3768.1>.
- , —, and R. E. Carbone, 2014: Mechanisms governing the persistence and diurnal cycle of a heavy rainfall corridor. *J. Atmos. Sci.*, **71**, 4102–4126, <https://doi.org/10.1175/JAS-D-14-0134.1>.
- , J. W. Wilson, D. A. Ahijevych, and R. A. Sobash, 2017: Mesoscale vertical motions near nocturnal convection initiation in PECAN. *Mon. Wea. Rev.*, **145**, 2919–2941, <https://doi.org/10.1175/MWR-D-17-0005.1>.
- Tsuda, T., T. E. VanZandt, M. Mizumoto, S. Kato, and S. Fukao, 1991: Spectral analysis of temperature and Brunt-Väisälä frequency fluctuations observed by radiosondes. *J. Geophys. Res.*, **96**, 17 265–17 278, <https://doi.org/10.1029/91JD01944>.
- Tuttle, J. D., and C. A. Davis, 2006: Corridors of warm season precipitation in the central United States. *Mon. Wea. Rev.*, **134**, 2297–2317, <https://doi.org/10.1175/MWR3188.1>.
- UCAR/NCAR–Earth Observing Laboratory, 2016a: FP3 NCAR/EOL water vapor DIAL, QC data in netCDF, version 2.0. UCAR/NCAR–Earth Observing Laboratory, accessed 2 March 2016, <https://doi.org/10.5065/D6SJ1HR1>.
- , 2016b: FP5 NCAR/EOL ISS QC 915 MHz profiler 30-minute consensus winds and moments data, version 1.0. UCAR/NCAR–Earth Observing Laboratory, accessed 11 July 2016, <https://doi.org/10.5065/D6H993DQ>.
- , 2016c: FP5 NCAR/EOL QC soundings version 2.0. UCAR/NCAR–Earth Observing Laboratory, accessed 5 October 2016, <https://doi.org/10.5065/D6ZG6QF7>.
- , 2016d: Radar regional 3D mosaic in netCDF format, DBZ and ZDR, version 1.0. UCAR/NCAR–Earth Observing Laboratory, accessed 7 November 2017, <https://doi.org/10.5065/D6QR4VHM>.

- Vermeesch, K., 2015: FP2 Greensburg, KS radiosonde data, version 1.0. UCAR/NCAR–Earth Observing Laboratory, accessed 18 April 2016, <https://doi.org/10.5065/D6FQ9TPH>.
- Wallace, J. M., 1975: Diurnal variations in precipitation and thunderstorm frequency over the continuous United States. *Mon. Wea. Rev.*, **103**, 406–419, [https://doi.org/10.1175/1520-0493\(1975\)103<0406:DVIPAT>2.0.CO;2](https://doi.org/10.1175/1520-0493(1975)103<0406:DVIPAT>2.0.CO;2).
- Walters, C. K., and J. A. Winkler, 2001: Airflow configurations of warm season southerly low-level wind maxima in the Great Plains. Part I: Spatial and temporal characteristics and relationship to convection. *Wea. Forecasting*, **16**, 513–530, [https://doi.org/10.1175/1520-0434\(2001\)016<0513:ACOWSS>2.0.CO;2](https://doi.org/10.1175/1520-0434(2001)016<0513:ACOWSS>2.0.CO;2).
- , —, R. P. Shadbolt, J. van Ravensway, and G. D. Bierly, 2008: A long-term climatology of southerly and northerly low-level jets for the central United States. *Ann. Assoc. Amer. Geogr.*, **98**, 521–552, <https://doi.org/10.1080/00045600802046387>.
- Weckwerth, T. M., and Coauthors, 2004: An overview of the International H<sub>2</sub>O Project (IHOP\_2002) and some preliminary highlights. *Bull. Amer. Meteor. Soc.*, **85**, 253–278, <https://doi.org/10.1175/BAMS-85-2-253>.
- Wilson, J. W., and R. D. Roberts, 2006: Summary of convective storm initiation and evolution during IHOP: Observational and modeling perspective. *Mon. Wea. Rev.*, **134**, 23–47, <https://doi.org/10.1175/MWR3069.1>.